

# Radio Structures of Seyfert Galaxies. VIII. A Distance and Magnitude Limited Sample of Early-Type Galaxies

Neil M. Nagar, Andrew S. Wilson

Department of Astronomy, University of Maryland, College Park, MD 20742;  
neil@astro.umd.edu, wilson@astro.umd.edu

John S. Mulchaey

Observatories of the Carnegie Institute of Washington, 813 Santa Barbara Street,  
Pasadena, CA 91101; mulchaey@ociw.edu

Jack F. Gallimore

Max-Planck Institut für extraterrestrische Physik, Postfach 1603, D-85740 Garching bei  
München, Germany; jfg@hethp.mpe-garching.mpg.de

**To appear in ApJS, Vol. 120 #2, February 1999**

## ABSTRACT

The VLA has been used at 3.6 and 20 cm to image a sample of about 50 early-type Seyfert galaxies with recessional velocities less than  $7,000 \text{ km s}^{-1}$  and total visual magnitude less than 14.5. Emission-line ([OIII] and  $\text{H}\alpha + [\text{NII}]$ ) and continuum (green and red) imaging of this sample has been presented in a previous paper. In this paper, we present the radio results, discuss statistical relationships between the radio and other properties and investigate these relationships within the context of unified models of Seyferts. The mean radio luminosities of early-type Seyfert 1's (i.e. Seyfert 1.0's, 1.2's and 1.5's) and Seyfert 2.0's are found to be similar (consistent with the unified scheme) and the radio luminosity is independent of morphological type within this sample. The fraction of resolved radio sources is larger in the Seyfert 2.0's (93%) than in the Seyfert 1's (64%). However, the mean radio extents of Seyfert 2.0's and Seyfert 1's are not significantly different, though this result is limited by the small number of resolved Seyfert 1's.

The nuclear radio structures of Seyfert 2.0's in the early-type sample tend to be aligned with the [OIII] and  $\text{H}\alpha + [\text{NII}]$  structures even though the radio extents are smaller than the [OIII] and  $\text{H}\alpha + [\text{NII}]$  extents by a factor of  $\sim 2 - >5$ . This alignment, previously known for individual Seyferts with 'linear' radio sources, is here shown to be characteristic of early-type Seyfert galaxies as a

class. Seyfert 2.0's in the early-type sample also show a significant alignment between the emission-line ( $[\text{OIII}]$  and  $\text{H}\alpha + [\text{NII}]$ ) axes and the major axis of the host galaxy. These alignments are consistent with a picture in which the ionized gas represents ambient gas predominantly co-planar with the galaxy stellar disk. This ambient gas is ionized by nuclear radiation that may escape preferentially along and around the radio axis, and is compressed in shocks driven by the radio ejecta. We use this alignment to constrain the product of the velocity of the radio ejecta and the period of any large angle precession of the inner accretion disk and jet :  $V_{\text{ejecta}} \times P \geq 2 \text{ kpc}$ .

An investigation of a larger sample of Seyferts reveals the unexpected result that the Seyfert 1's with the largest radio extent ( $\geq 1.5 \text{ kpc}$ ) are all of type Seyfert 1.2. It appears that classification as this type of intermediate Seyfert depends on some factor other than the relative orientation of the nuclear obscuring torus to the line of sight. Among all the other Seyferts, the distribution of radio extent with Seyfert intermediate type is consistent with the expectations of the unified scheme.

*Subject headings:* galaxies: nuclei — galaxies: Seyfert — radio continuum: galaxies — galaxies: structure — surveys

## 1. Introduction

Centimeter wave emission from active galactic nuclei (AGN) is unaffected by the extinction that plagues some other wavebands and can be imaged at high ( $\lesssim 1''$ ) spatial resolution with instruments like the Very Large Array (VLA). These two factors can be exploited to provide important clues towards an understanding of the workings of their central engines.

A number of samples of Seyfert galaxies have been observed at resolutions  $\lesssim 1''$  with the VLA. A radio flux-limited sample of Markarian Seyferts was studied by Ulvestad & Wilson (1984a, hereafter Paper V). A distance-limited sample, comprising the 57 Seyfert galaxies known as of mid-1983 with recession velocity less than  $4,600 \text{ km s}^{-1}$  and declination  $> -45^\circ$ , was mapped by Ulvestad & Wilson (1984b, hereafter Paper VI; 1989, hereafter Paper VII). More recently, Kukula et al. (1995) have imaged 46 of the 48 Seyferts in a magnitude-limited ( $m_{pg} < 14.5$ ) sample (the CfA Seyfert sample). Together, these samples represent less than 15% of all known Seyferts. Lower spatial resolution radio surveys have also been completed e.g. the CfA (Edelson 1987) and the  $12\mu\text{m}$  Seyfert galaxy samples

(Rush, Malkan & Edelson 1996). However, lower resolution surveys are contaminated by disk radio emission and thus do not provide direct information on nuclear properties.

These surveys have largely supported the unified model (see Antonucci 1993, Urry & Padovani 1995 for reviews) of AGN. Ulvestad & Wilson (Paper VII) concluded that the trend for Seyfert 2 galaxies to have stronger and larger radio sources (found in Papers V and VI) is only marginally statistically significant. Giuricin et al. (1990) also found no clear evidence for a significant difference in the major radio properties (radio luminosity, radio-to-optical luminosity, radio spectral index, and radio size) of Seyfert 1's and Seyfert 2's, while Rush et al. (1996) showed that there is no significant difference between the average 6–20 cm spectral indices of Seyfert 1's and Seyfert 2's. Interestingly, Edelson (1987) found that while there is no significant difference between the radio luminosities of Seyfert 1 and Seyfert 2 galaxies, the normalized radio to total optical luminosity of Seyfert 2 galaxies is greater than that of Seyfert 1 galaxies by a factor of  $\simeq 2$ , at a 99% confidence level.

The radio properties of Seyferts are also relevant to the excitation and properties of the narrow line region. The radio luminosities are known to be correlated with both the narrow emission-line luminosities (de Bruyn & Wilson 1978; Whittle 1985, 1992c) and the narrow emission-line widths (Wilson & Willis 1980; Whittle 1985, 1992b). Recent high resolution imaging (using HST and the VLA or MERLIN) shows a close spatial association between the radio and the high excitation gas structures in almost all Seyfert 2's studied (Bower et al. 1994, 1995; Capetti et al. 1996; Falcke, Wilson & Simpson 1998). Capetti et al. (1996) and Falcke et al. (1998) find strong evidence that the line-emitting gas is compressed by the shocks created by the passage of the radio-emitting outflow; the interaction increases the ambient density, causing increased line emission. They also find that radio lobes produce emission-line gas in shell or bow-shock like morphologies formed by the sweeping up of material by the ejected and expanding lobes, while radio jets produce linear emission-line structures, perhaps formed by the lateral expansion of hot gas around the jet axis. The radio and 'ionization cone' axes are also closely correlated (Wilson & Tsvetanov 1994) implying that photons from the central engine escape preferentially along the radio axis, a model originally indicated by the fact that high excitation ionized gas is detected well beyond the inner radio lobes (Unger et al. 1987b).

Mulchaey, Wilson & Tsvetanov (1996a, hereafter MWZ) have reported an optical imaging survey of a sample of 57 early-type Seyfert galaxies; the galaxies were imaged in  $[\text{OIII}]\lambda 5007$ ,  $\text{H}\alpha$  +  $[\text{NII}]\lambda\lambda 6548, 6583$  and the nearby continua (green and red). The motivation for choosing early-type Seyferts came from Haniff, Ward & Wilson (1991) who found that most clearly defined extended, high excitation nebulosities are preferentially found in Seyfert galaxies of type S0. Almost all of the galaxies studied by MWZ showed

extended emission in [OIII] and  $H\alpha + [NII]$ .

In the present paper, we present a high resolution radio survey of the early-type Seyfert galaxy sample of MWZ. We use the results to investigate unified models of Seyfert galaxies and the relationships between radio and emission-line properties and between emission-line structures and the host galaxies. A separate paper (Nagar & Wilson 1998) discusses the orientations of the radio ejecta of Seyfert nuclei with respect to their host galaxy disks. For consistency with MWZ and with earlier papers in this series, all distance-dependent quantities have been calculated from recessional velocities assuming  $H_0 = 50 \text{ km s}^{-1} \text{ Mpc}^{-1}$ . We use [OIII] to denote the [OIII]  $\lambda 5007$  line, and  $H\alpha + [NII]$  to denote  $H\alpha + [NII] \lambda\lambda 6548, 6583$ . We use ‘Seyfert 1’ to denote Seyfert 1.0 through Seyfert 1.5, and treat Seyfert 1.8’s and Seyfert 1.9’s independently of Seyfert 2.0’s (‘Seyfert 2.0’ emphasizes that this class does not include Seyfert 1.8’s and Seyfert 1.9’s), as Maiolino & Rieke (1995) present evidence that Seyfert 1.8’s and 1.9’s are type 1 nuclei seen through a 100 pc-scale torus coplanar with the galaxy disk and not type 1 nuclei partially obscured by an inner pc-scale torus.

We have made extensive use of the following catalogs and databases - “Third Reference Catalogue of Bright Galaxies” (de Vaucouleurs et al. 1991, hereafter RC3), “Uppsala General Catalogue of Galaxies” (Nilson 1973, hereafter UGC), “ESO/Uppsala Survey of the ESO(B) Atlas” (Lauberts 1982, hereafter ESO), “Extended Southern Galactic Catalog” (Corwin et al. 1998, hereafter ESGC), “The NASA/IPAC Extragalactic Database” (see e.g. Helou et al. 1991, hereafter NED), “The Lyon-Meudon Extragalactic Database” (see e.g. Paturel et al. 1997, hereafter LEDA), and the STScI Digitized Sky Survey (hereafter DSS).

## 2. Sample and Observations

A detailed description of the early-type Seyfert sample selection and a discussion of its completeness can be found in MWZ and Mulchaey, Wilson & Tsvetanov (1996b). Briefly, Seyfert galaxies were selected from the catalogs of Hewitt & Burbidge (1991), Huchra (1989), & Veřon-Cetty and Veřon (1991). All Seyferts with total magnitude  $m_V \leq 14.5$ , recessional velocity  $cz < 7,000 \text{ km s}^{-1}$  and morphological type E, S0 or S0/a were included in the MWZ early-type “Sample I.” Our radio sample consists of all galaxies in this sample that are north of declination  $\delta = -41^\circ$  and an additional 3 objects (NGC 7743, Mkn 335 and Mkn 612) later found to satisfy the selection criterion. The final early-type sample for which statistical studies are reported in Section 5 therefore consists of 43 Seyfert galaxies; 14 Seyfert 1’s, 2 Seyfert 1.9’s and 27 Seyfert 2.0’s.

New radio observations of 47 galaxies were made in the A- and A/B-hybrid configurations of the VLA between December 1992 and February 1993 (see e.g. Thompson et al. 1980 for a description of the VLA configurations). These 47 galaxies comprise the early-type Seyfert sample of 43, minus two galaxies (MCG–5-23-16 and Mrk 1239) which were not re-observed as high resolution VLA maps exist in the literature (Paper VI and Ulvestad, Antonucci & Goodrich 1995), plus four misclassified Seyferts (Mrk 938, Mrk 565, Mrk 577 and NGC 5077), and two Seyferts not included in the sample studied in Section 5 (Mrk 10, host galaxy of morphological type Sb and NGC 6251, a radio-loud object). Each source was observed consecutively at L (20 cm) and X (3.6 cm) band (central frequencies 1465 MHz and 8440 MHz, respectively). Two galaxies, Mrk 10 and NGC 513, were observed at only L band. The time spent on each source was typically 15 to 20 min in each band. Source observations were sandwiched between two 1 min observations of a nearby calibrator. The two sets of VLA intermediate frequency (IF) channels used gave a total bandwidth of 100 MHz at each band. Data from the two sets of IF’s were calibrated separately and then combined and mapped. Observations of 0134+329 and 1328+307 were used to set the flux density scale to that of Baars et al. (1977). Most of the maps were made at the highest resolution possible (uniform weighting with Briggs’s robust parameter set to  $-4$  in the AIPS software). In some of the noisier maps, it was necessary to use either uniform weighting with a robust parameter of 0 or natural weighting to achieve better signal to noise at the expense of resolution. The stronger sources were iteratively self-calibrated and mapped. The r.m.s. noise in the final maps is typically 80 to 150  $\mu$ Jy for the 20 cm maps and 40 to 90  $\mu$ Jy for the 3.6 cm maps. The southern sources ( $\delta \lesssim -20^\circ$ ) have significantly larger noise values.

### 3. Results

In this section we present contour maps (Figures 1–15) for all the observed sources and tables (Tables 1–5) of derived source properties. Of the 47 galaxies observed, Mrk 577 was not detected at either 3.6 or 20 cm, which is not surprising as this is not a Seyfert galaxy (MWZ), and NGC 4117 was not detected at 3.6 cm. No useful data were obtained on MCG–2-27-9 at either 3.6 or 20 cm as the pointing center was incorrect by  $\sim 85''$ . A cross marks the optical position of the galaxy on the contour map whenever this position falls within the field of view of the radio map. In the 3.6 cm maps, the semi-length of the arms of the cross represents the error in the position of the optical nucleus. In the 20 cm maps, we use a minimum cross size of  $1''$  in order to keep the cross visible. Most optical positions and errors are taken from Clements (1981; 1983) and Argyle & Eldridge (1990); these positions have typical internal errors of  $\pm 0'.1 - 0'.2$ . Radio positions and

flux densities of most unresolved or slightly resolved components have been determined by Gaussian model fitting. In the case of more extended components, the position of the flux maximum is given. For such extended structure, or for slightly resolved sources for which Gaussian model fitting is inappropriate, the flux has been summed within a box containing all significant emission.

Table 1 summarizes the properties of all the 47 galaxies which have been newly observed with the VLA plus the two additional galaxies in the early-type radio sample that have been previously observed with the VLA (Section 2). The leftmost columns in Table 1 are as follows : (1) galaxy name; (2) other common name; (3) and (4) radio position (B1950). When more than one radio component is present, the position listed was determined as follows. If a component appears on both the 3.6 and 20 cm maps, we give its position. If more than one component satisfies this criterion, we have listed the position of the strongest one. If multiple components have similar strengths, the component closest to the optical position is listed. The other columns of Table 1 are : (5) host galaxy type from the RC3 or UGC catalog; (6) Seyfert type. If broad permitted lines are present we follow, whenever possible, the Seyfert classification scheme adopted by Whittle (1992a) which is based on the flux ratio  $R = F_{[OIII]} / F_{H\beta}$ , where  $F_{[OIII]}$  is the [OIII] flux and  $F_{H\beta}$  the total (broad plus narrow)  $H\beta$  flux. These types are (with  $R$  values) Sey 1.0 ( $R \leq 0.3$ ), Sey 1.2 ( $0.3 < R \leq 1$ ), Sey 1.5 ( $1 < R \leq 4$ ), Sey 1.8 ( $R > 4$ ) and Sey 1.9 (assigned if only broad  $H\alpha$  is seen). As in Whittle (1992a), some Seyferts with highly variable  $H\beta$  flux are classified as Sey 1.5. We have used emission-line fluxes listed in Whittle (1992a) and Winkler (1992); for objects for which we could find no measurement of  $R$ , we use the classification given in NED. The source of the Seyfert classification for galaxies with broad permitted lines can be found in the comments column (column 13); (7) radio structure, where, as in Paper V: L = linear; D = diffuse; A = ambiguous; S = slightly resolved; and U = unresolved. Single component sources which, after Gaussian deconvolution, are larger than one half the beam size are considered ‘S’. These sources are  $> 1.12$  times the beam size before deconvolution. Sources which, after Gaussian deconvolution, were smaller than one half the beam size, but showed clear signs of an extension in either the 3.6 cm or 20 cm contour maps are tentatively considered to be slightly resolved and are listed as ‘(S)’. Similarly, multi-component sources with apparently ‘linear’ structure in which the reality of the weaker components is not completely certain, are listed as ‘(L)’; (8) total flux from all components at 3.6 cm; (9) total flux from all components at 20 cm; (10) largest linear extent (in kpc) of the radio emission in the 3.6 and 20 cm maps. For unresolved sources, two numbers are listed, representing an upper limit of half the beam size at 3.6 and 20 cm, respectively. For slightly resolved sources, we use the source size after Gaussian deconvolution. For sources with multiple unresolved components, we use the peak to peak

distance between the most widely separated components. The extents for “(S)” and “(L)” sources have been measured assuming that the extensions are real and these values are listed in brackets; (11) host galaxy morphological type (Hubble T parameter), taken from the RC3 or UGC catalogs unless otherwise mentioned. The uncertainty in T, if listed in the catalog, is given in brackets; (12) heliocentric recessional velocity of the galaxy taken from NED; (13) comments according to the key at the bottom of the table.

Table 2 lists the positions and fluxes of each component for all multiple component sources. Components have been named according to apparent morphology e.g. ‘Core’, ‘Ext’ (Extended), ‘Center’, ‘Jet’, ‘Arm’, and/or by direction. In several cases, multiple components in the 3.6 cm map cannot be spatially separated in the 20 cm map. The total 20 cm flux of these components is then listed opposite the first of these components and the 20 cm flux of the other component(s) is left blank.

Table 3 lists relevant major axis position angles (P.A.’s), in degrees, of various structures for all galaxies in the early-type radio sample that are resolved in the radio. All P.A.’s are measured north through east, with  $0^\circ \leq \text{P.A.} \leq 180^\circ$ . In order to provide a measure of their reliability, each of the radio P.A.’s and the galaxy major axis P.A.’s are assigned a quality flag - ‘a’ (highest quality) through ‘d’ (lowest quality). An explanation of the flags is given in Table 4; a more detailed discussion on the reasons for choosing the specific limits for each quality flag can be found in Nagar & Wilson (1998). The columns of Table 3 are : (1) name; (2) Seyfert type; (3) P.A. in 3.6 cm map published in this paper and its quality flag; (4) P.A. in 20 cm map published in this paper and its quality flag; (5) adopted radio P.A., derived from column (3) and (4) or from the literature, and its quality flag. When curved structure is present, the P.A. of the smallest scale extension is listed; (6) and (7) P.A. of the [OIII] emission and the  $\text{H}\alpha + [\text{NII}]$  emission at a surface brightness of  $2 \times 10^{-16} \text{ ergs cm}^{-2} \text{ s}^{-1} (\text{arcsec})^{-2}$ , from MWZ. This is the level of the lowest contour in the images of MWZ. Typical errors are  $\pm 10^\circ$  and values in brackets have higher uncertainties. (8) P.A. of the green continuum emission at a surface brightness of  $2 \times 10^{-18} \text{ ergs cm}^{-2} \text{ s}^{-1} \text{ \AA}^{-1} (\text{arcsec})^{-2}$ , from MWZ. This is the level of the lowest contour in the images of MWZ. Typical errors are  $\pm 5^\circ$  and values in brackets have larger uncertainties. (9) P.A. of the major axis of the host galaxy, obtained as indicated in column 10, and our adopted quality flag. It is notable that, when the major axis of the galaxy is determined photometrically, it is measured at an extent which is typically  $\geq 2$  times that at which the green continuum P.A. is measured; (10) comments according to the key at the bottom of the table. The r.m.s. noise and the contour levels (in multiples of the r.m.s. noise) of each map (Figures 1–15) are listed in Table 5.

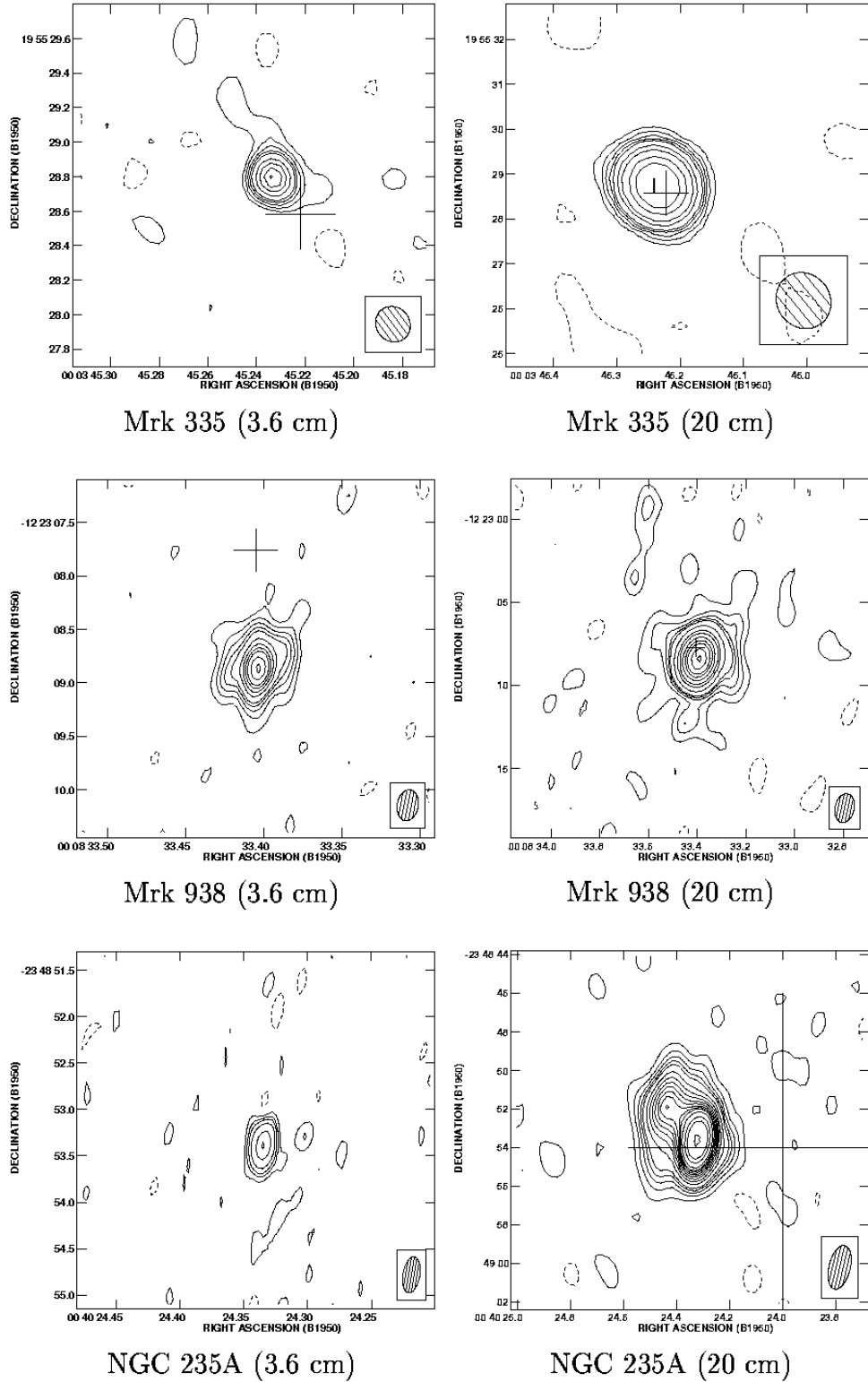


Fig. 1.— 3.6 cm and 20 cm VLA maps. See Table 5 for contour levels.



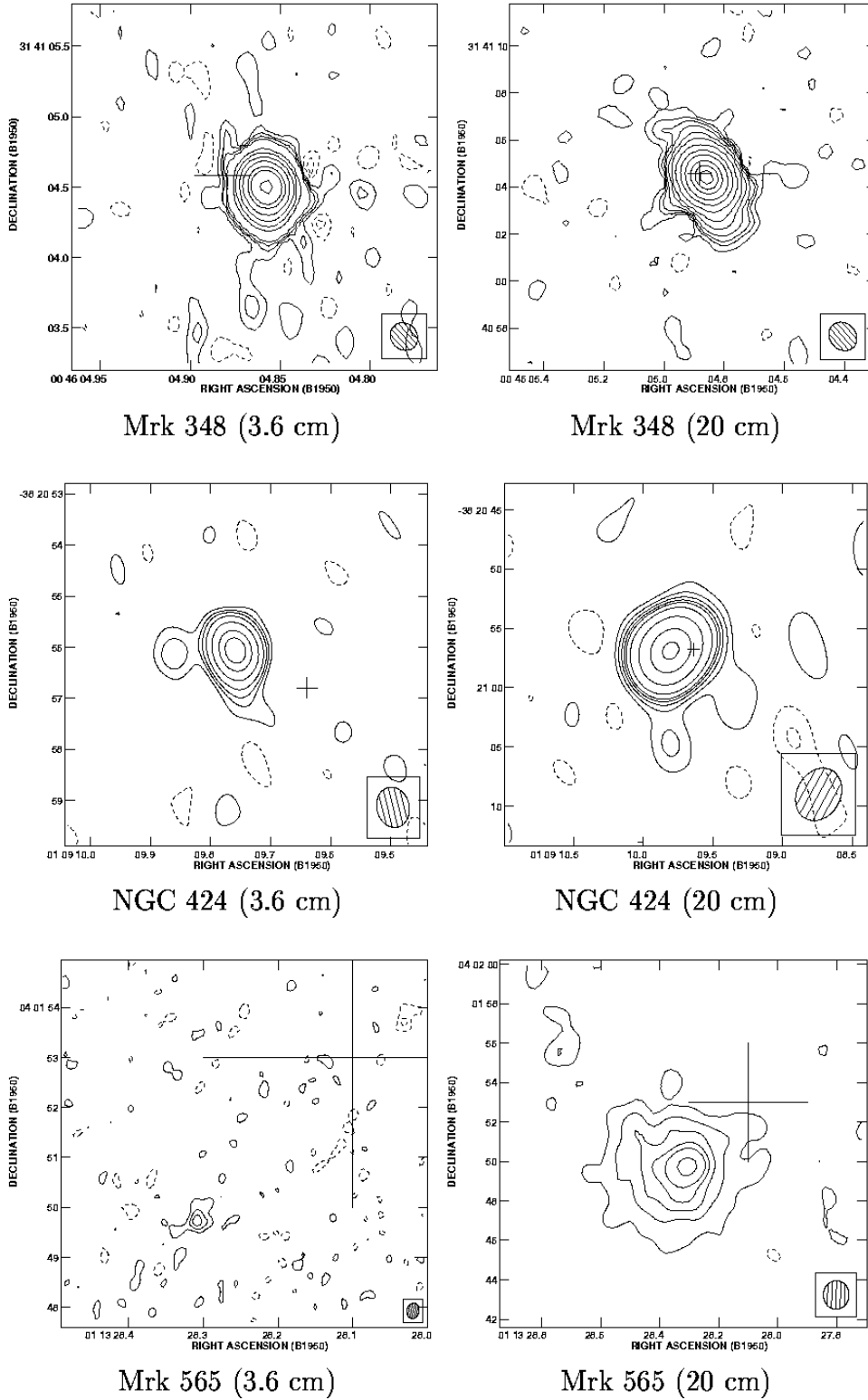
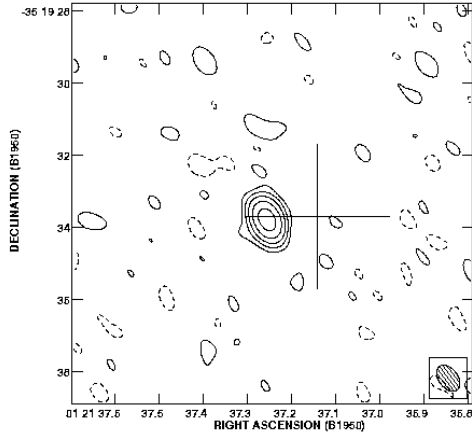
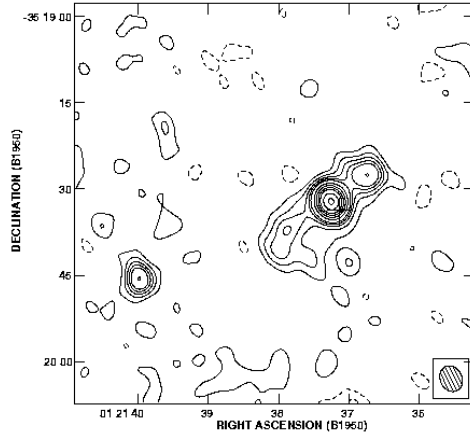


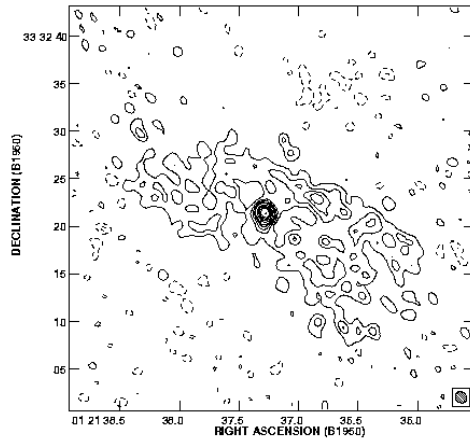
Fig. 2.— 3.6 cm and 20 cm VLA maps. See Table 5 for contour levels.



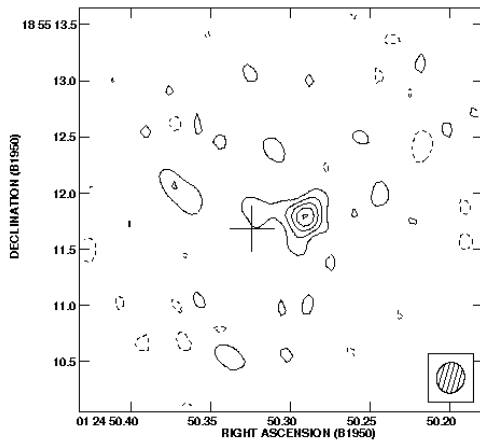
NGC 526A (3.6 cm)



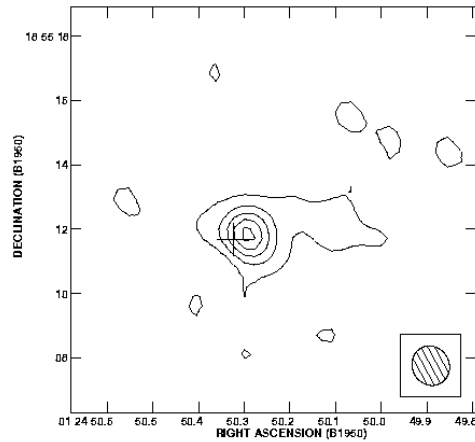
NGC 526A (20 cm)



NGC 513 (20 cm)



Mrk 359 (3.6 cm)



Mrk 359 (20 cm)

Fig. 3.— 3.6 cm and 20 cm VLA maps. See Table 5 for contour levels.

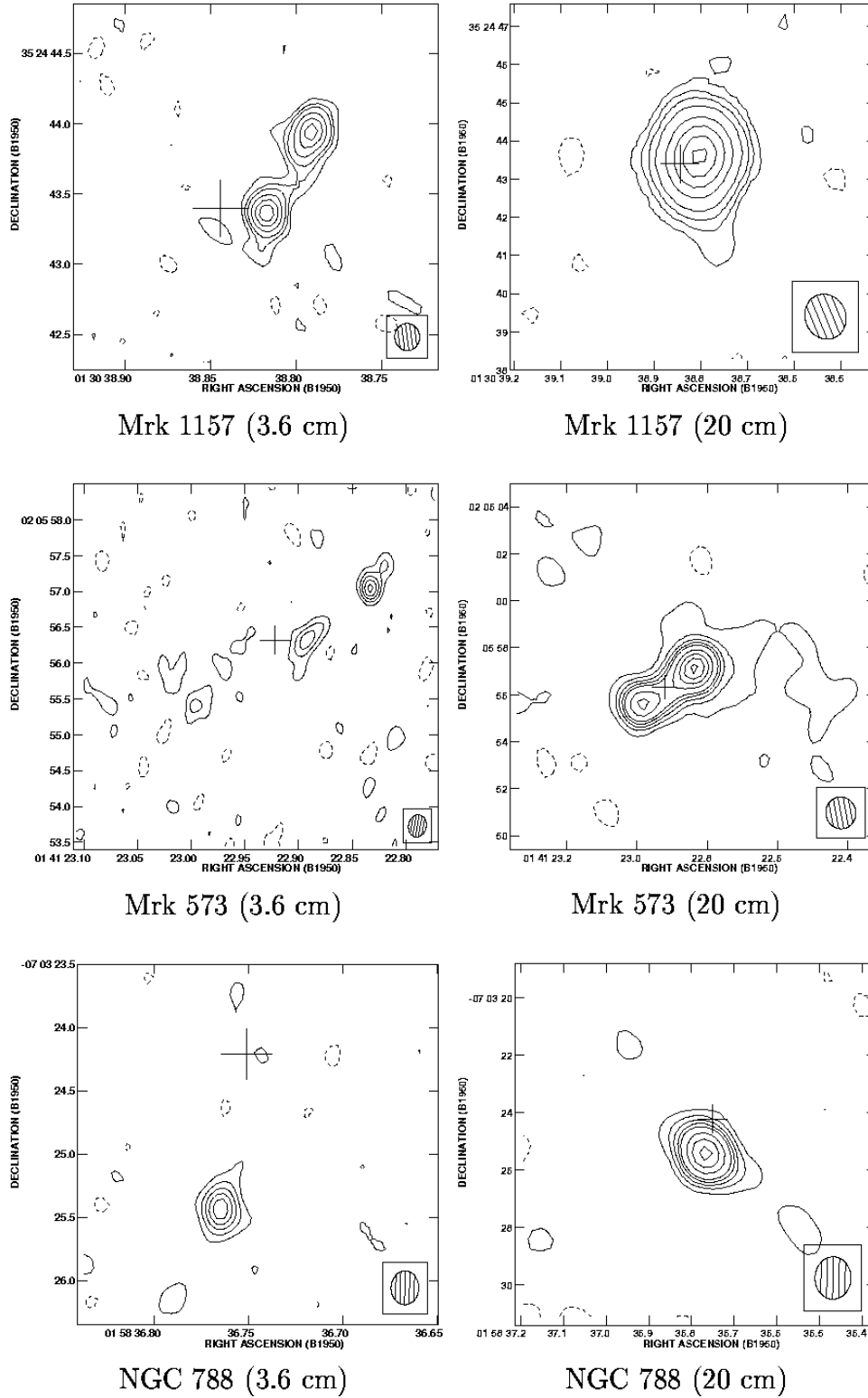


Fig. 4.— 3.6 cm and 20 cm VLA maps. See Table 5 for contour levels.

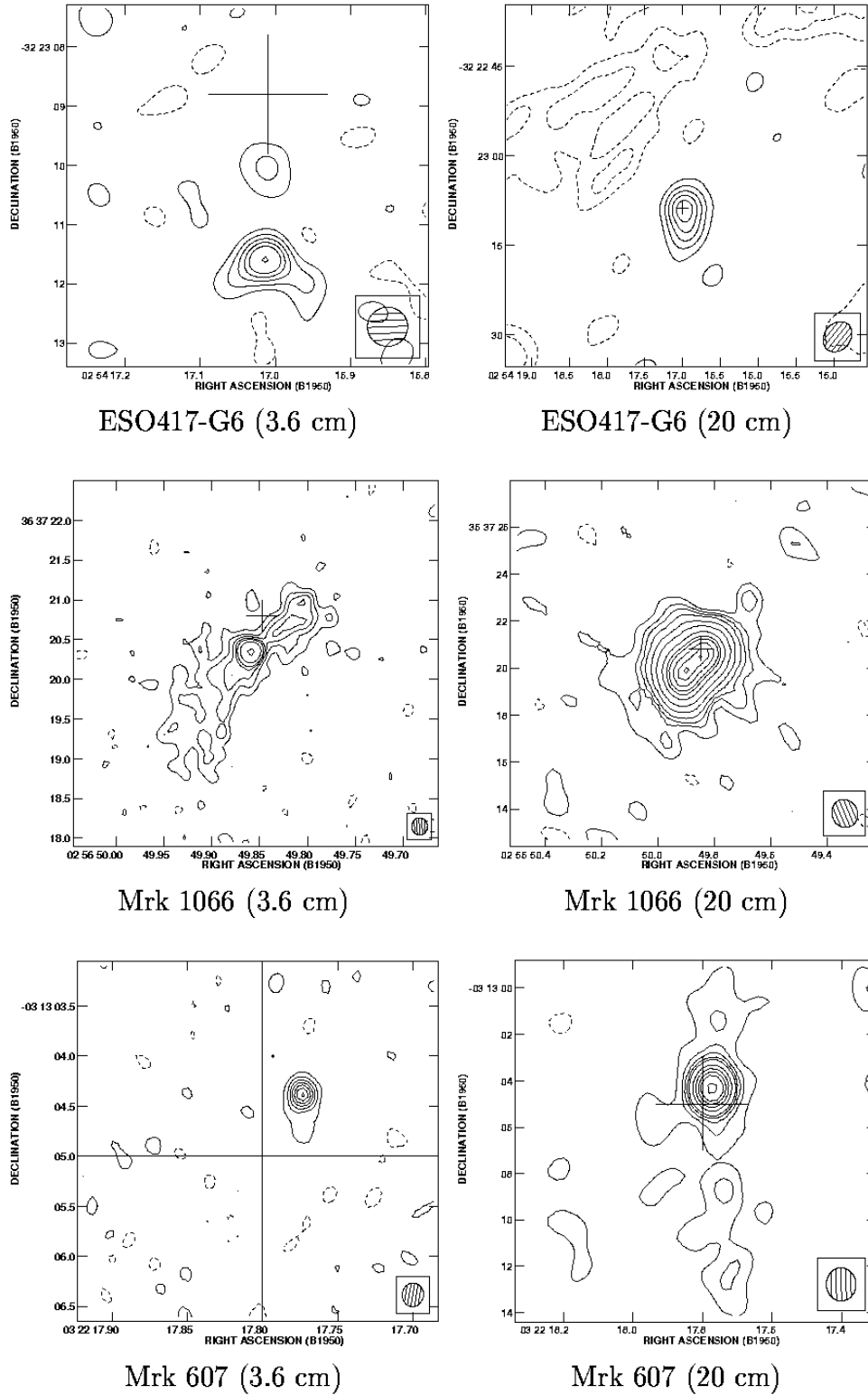


Fig. 5.— 3.6 cm and 20 cm VLA maps. See Table 5 for contour levels.

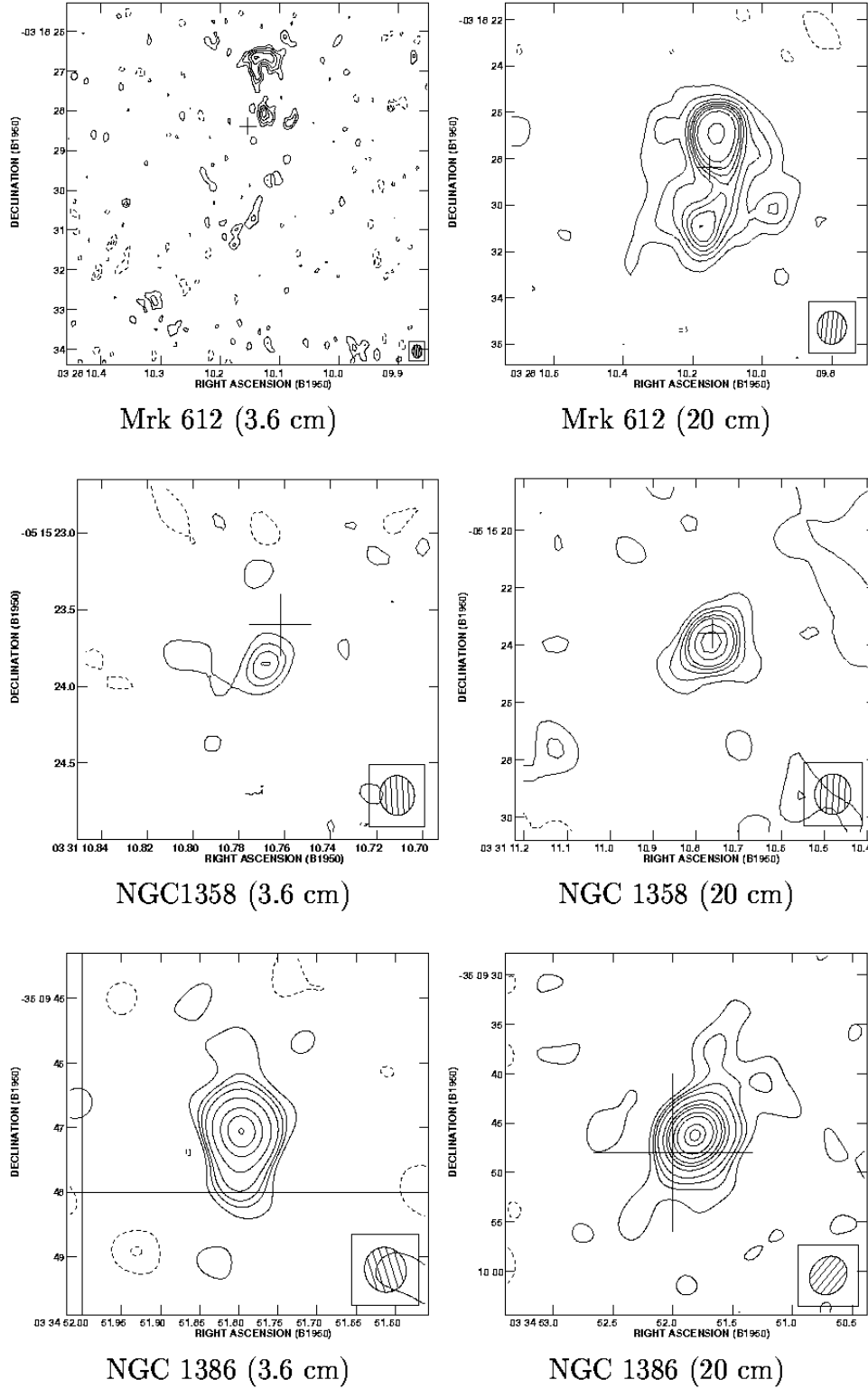


Fig. 6.— 3.6 cm and 20 cm VLA maps. See Table 5 for contour levels.

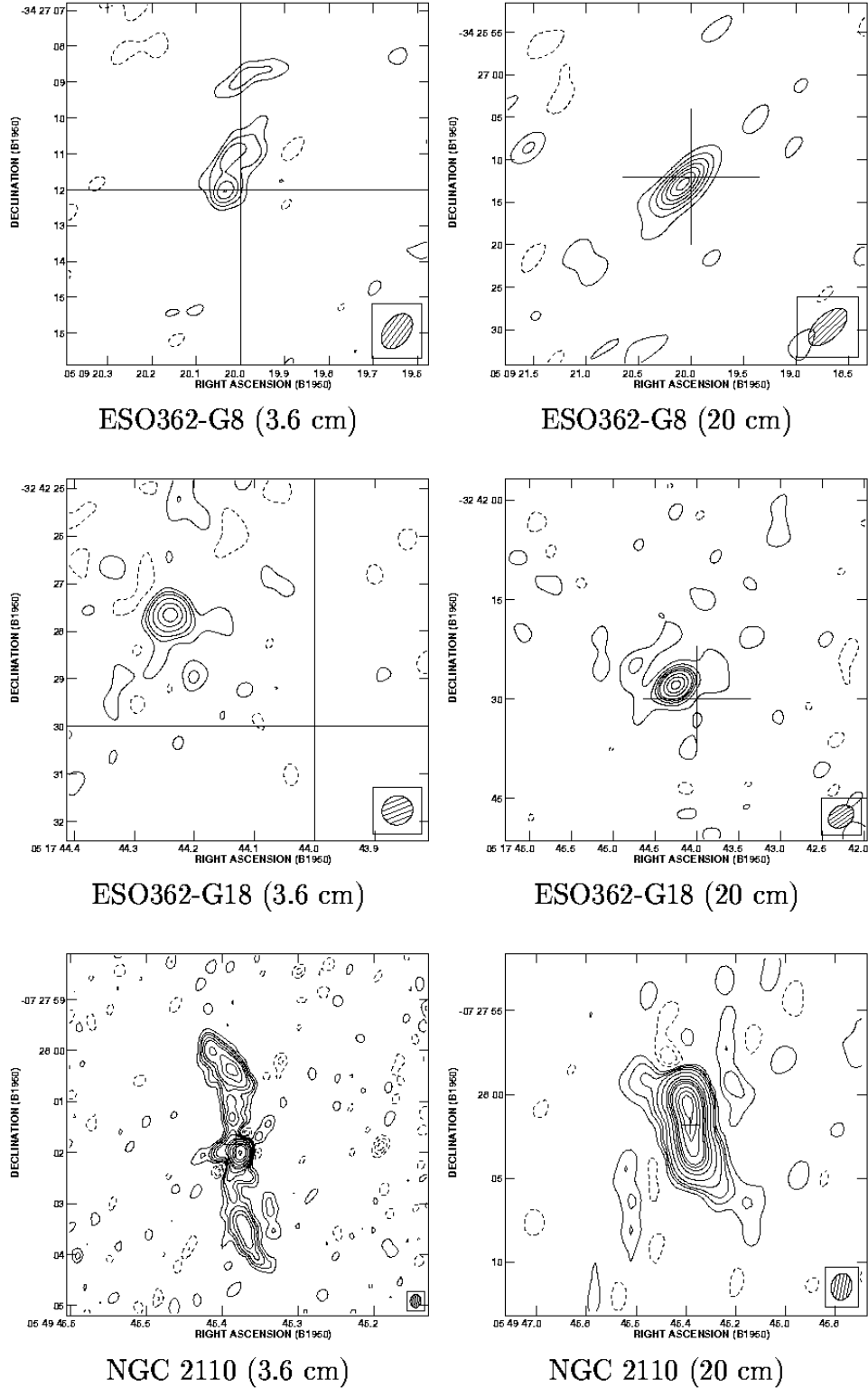


Fig. 7.— 3.6 cm and 20 cm VLA maps. See Table 5 for contour levels.

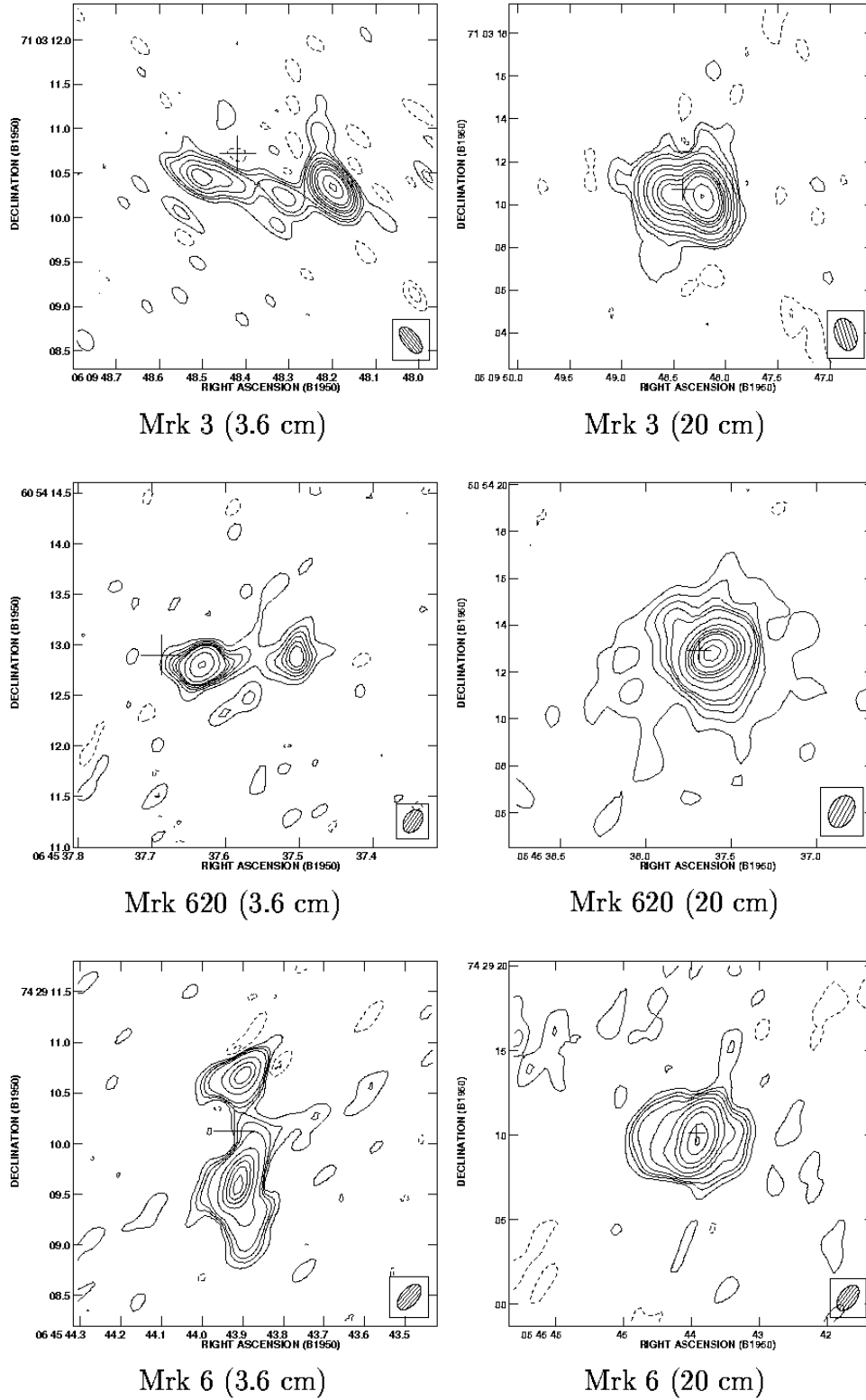


Fig. 8.— 3.6 cm and 20 cm VLA maps. See Table 5 for contour levels.

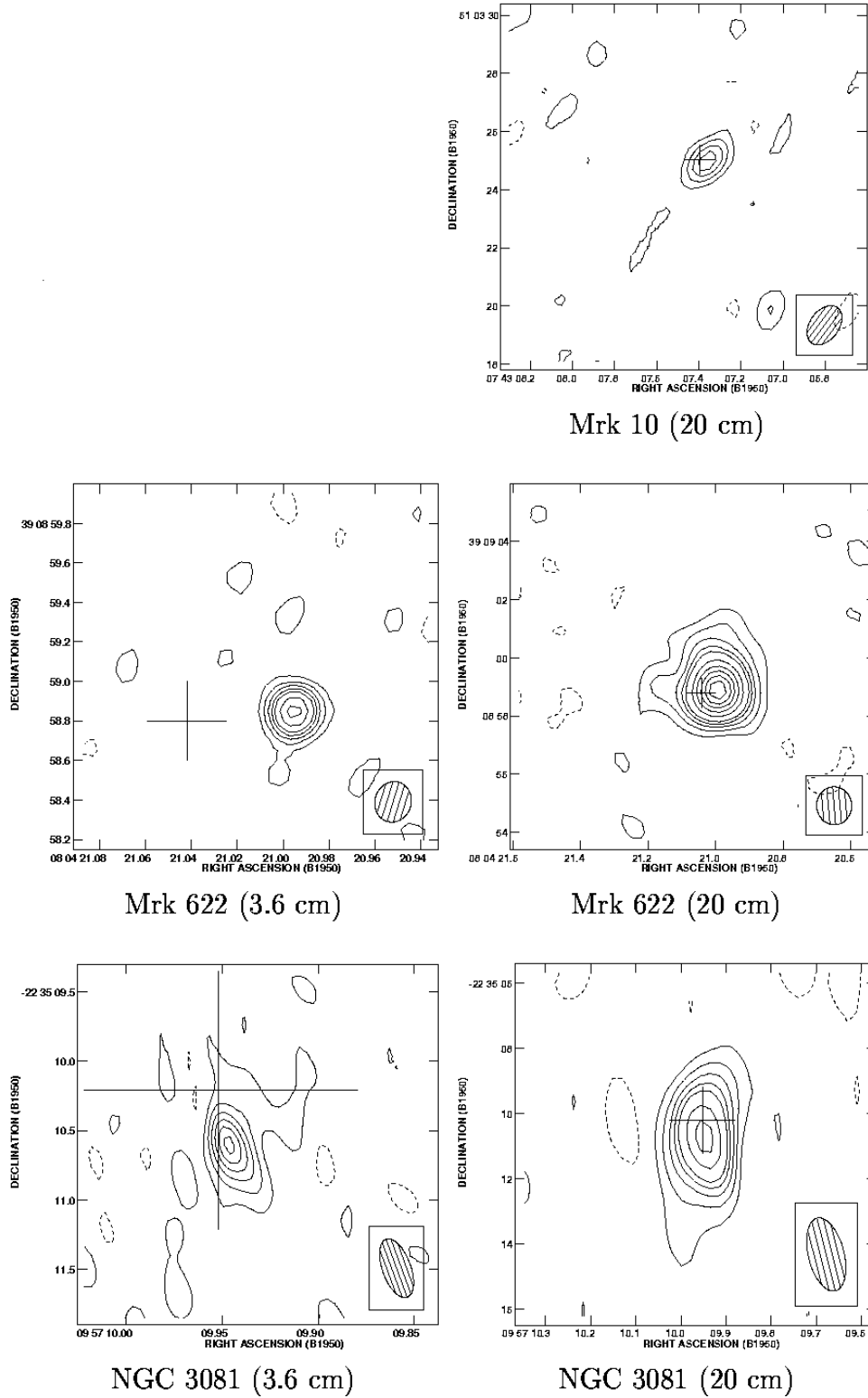


Fig. 9.— 3.6 cm and 20 cm VLA maps. See Table 5 for contour levels.



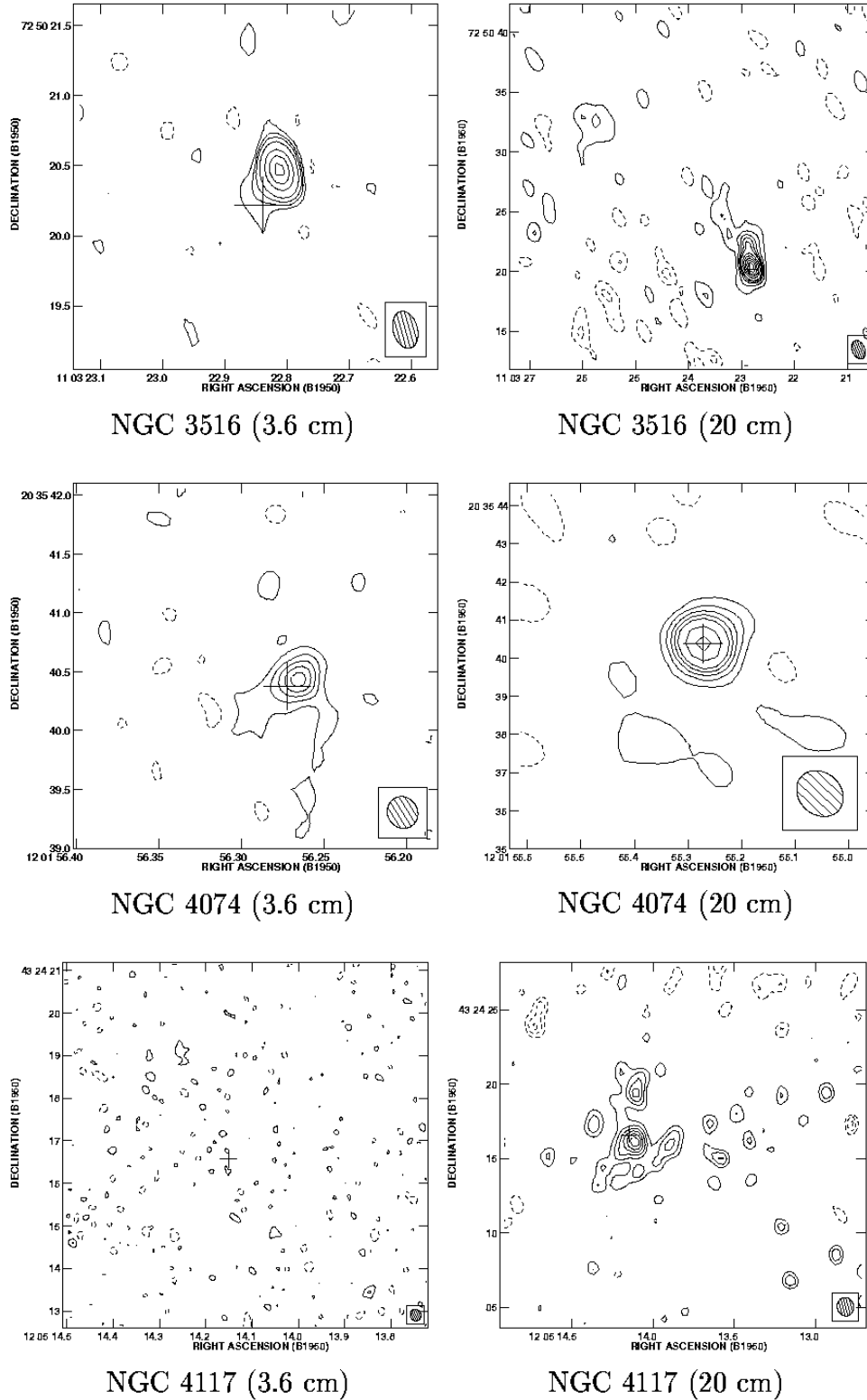


Fig. 10.— 3.6 cm and 20 cm VLA maps. See Table 5 for contour levels.

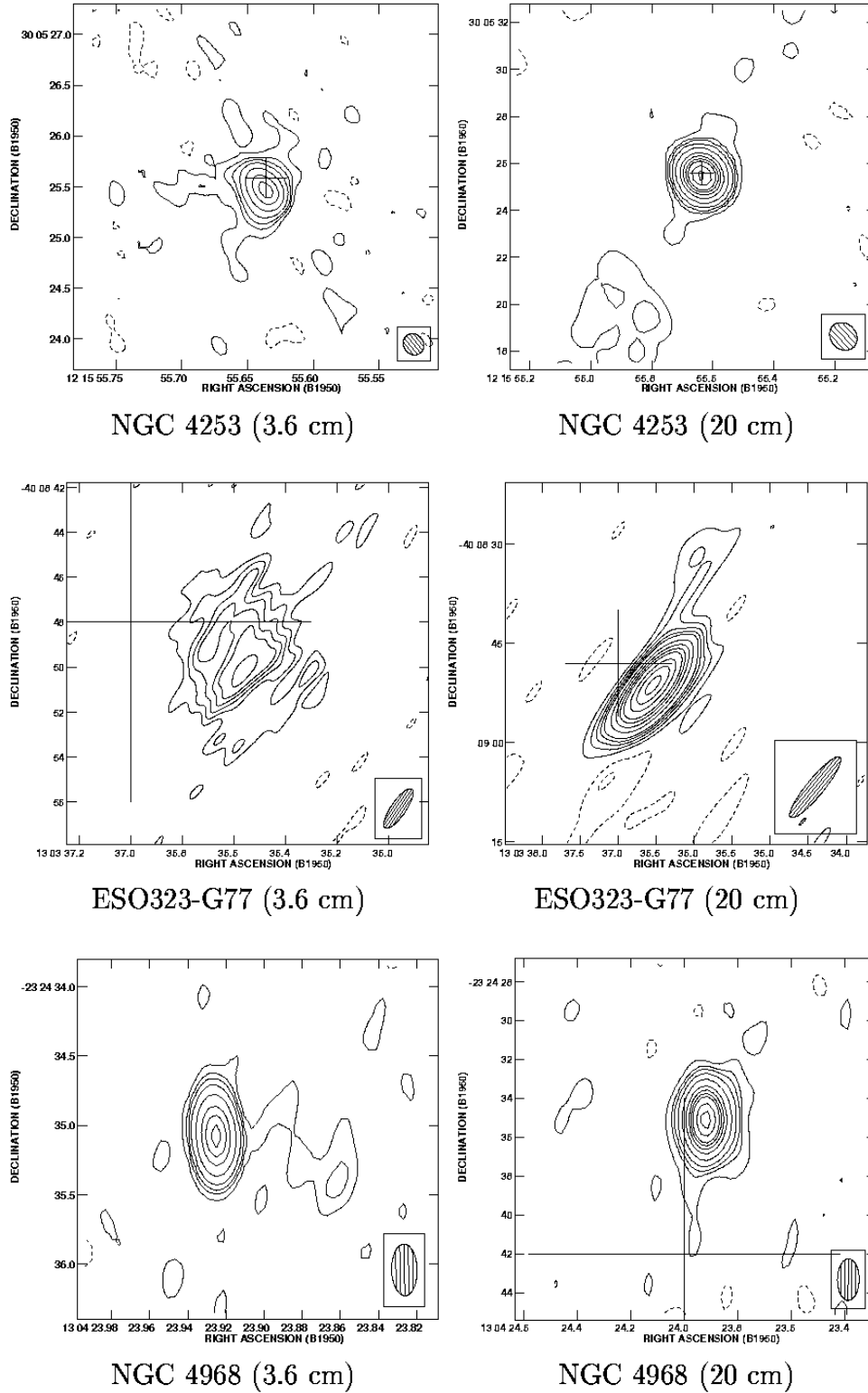


Fig. 11.— 3.6 cm and 20 cm VLA maps. See Table 5 for contour levels.

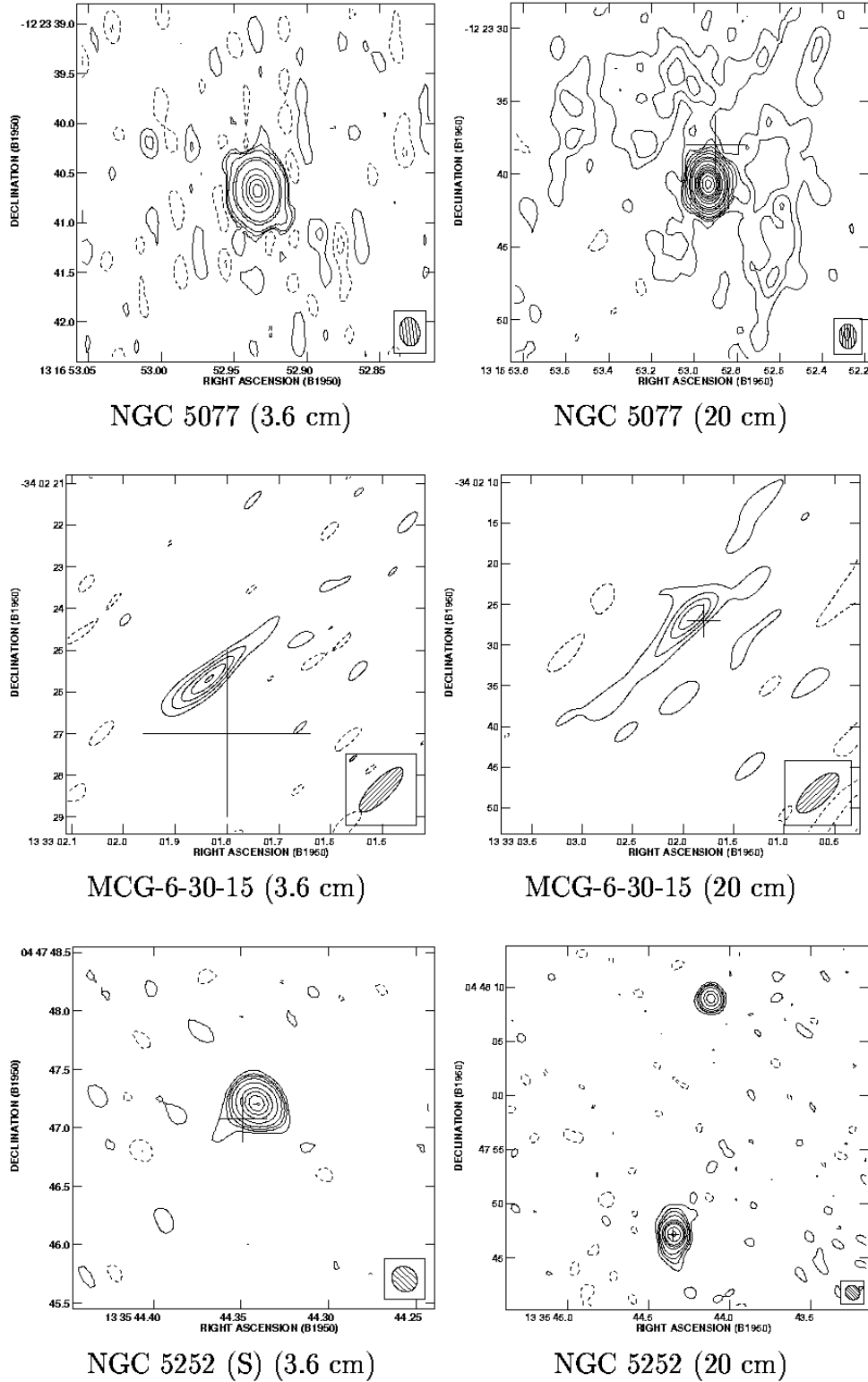


Fig. 12.— 3.6 cm and 20 cm VLA maps. See Table 5 for contour levels.

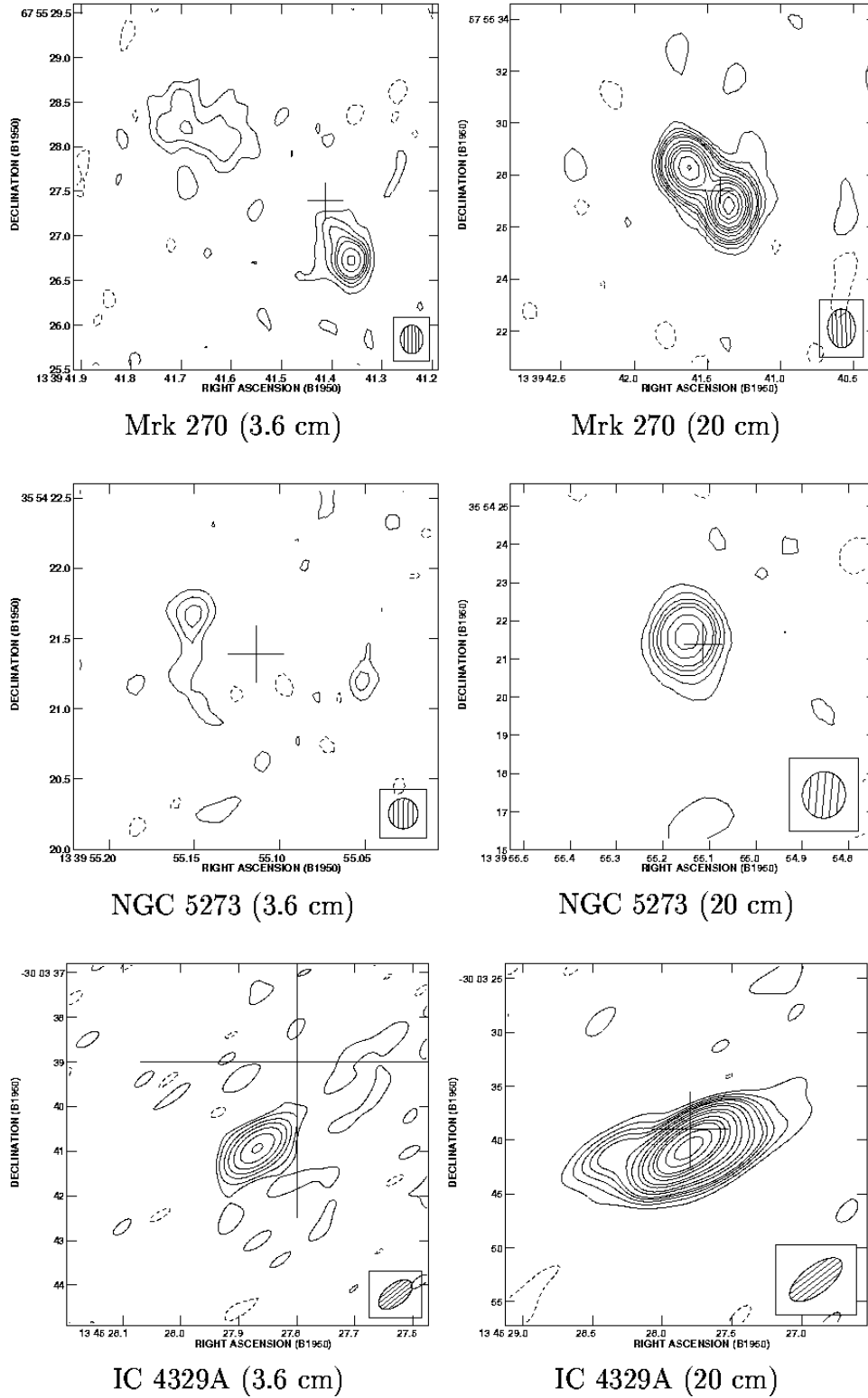


Fig. 13.— 3.6 cm and 20 cm VLA maps. See Table 5 for contour levels.

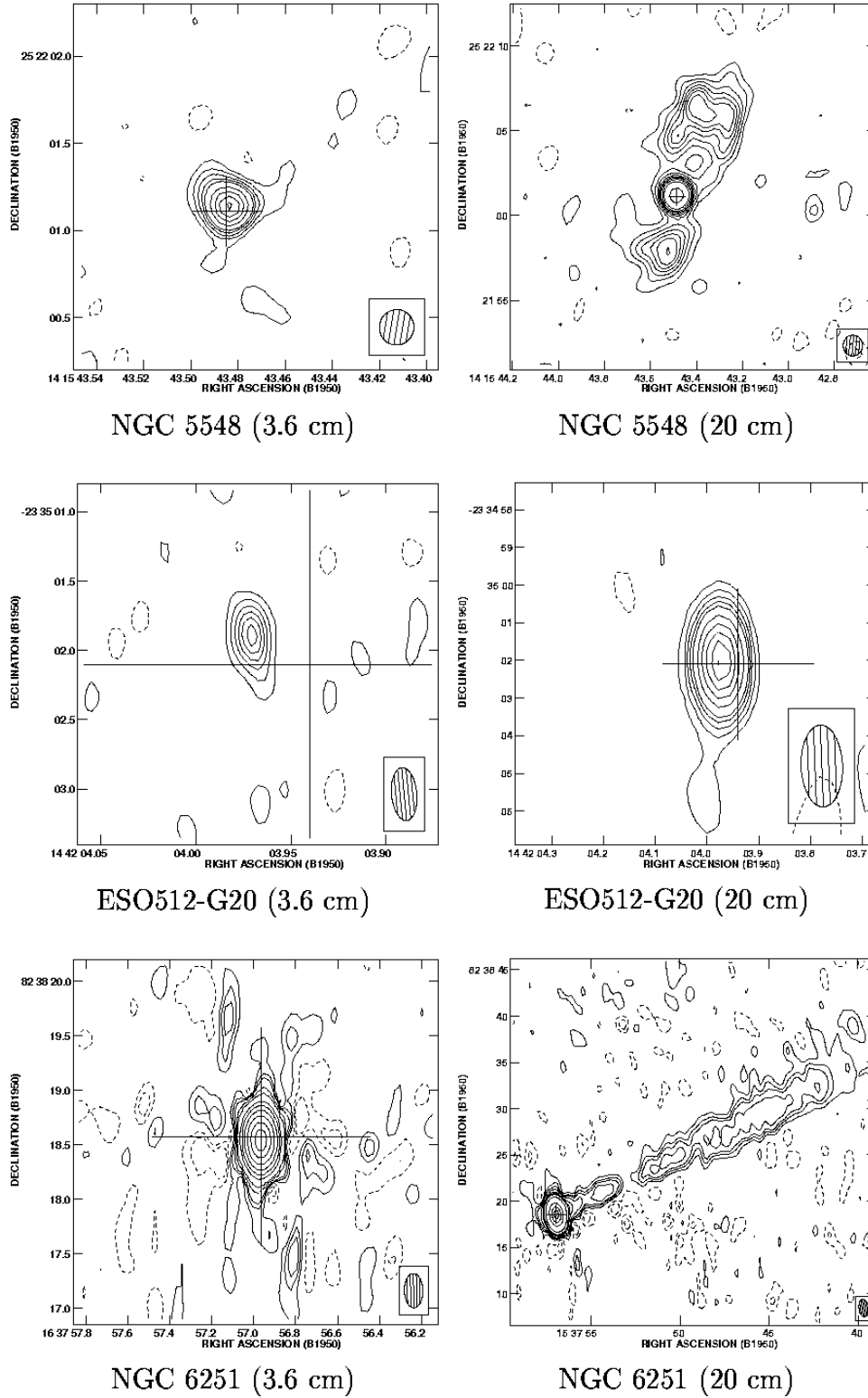


Fig. 14.— 3.6 cm and 20 cm VLA maps. See Table 5 for contour levels.

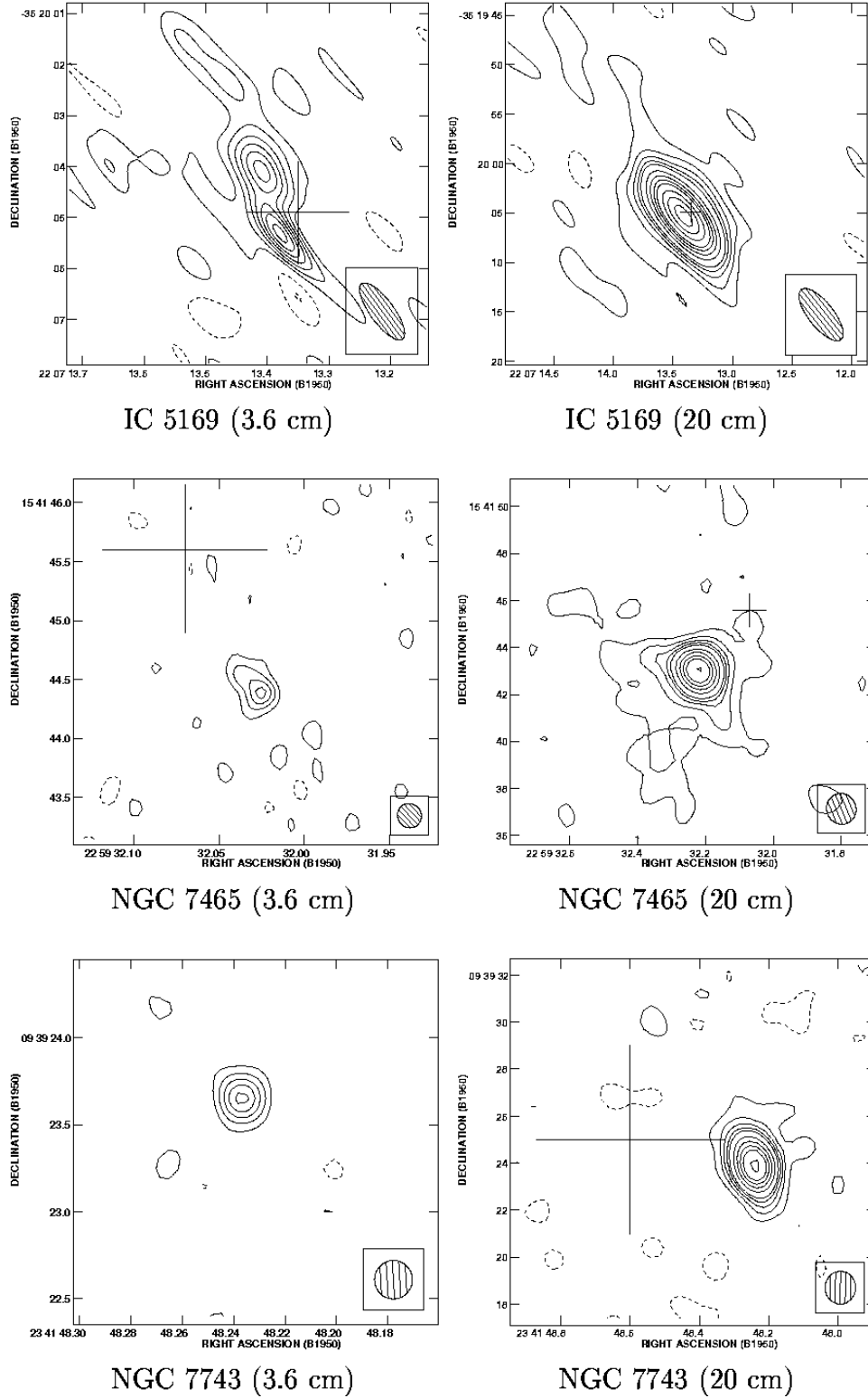


Fig. 15.— 3.6 cm and 20 cm VLA maps. See Table 5 for contour levels.

#### 4. Notes on individual objects

Comments on many individual galaxies are listed below. Further comments on the optical properties of most of the sources can be found in MWZ. A number of radio sources apparently unrelated to the Seyfert galaxy were detected in many of the maps. Most of these extraneous sources are far enough from the antenna pointing center that they are appreciably bandwidth smeared. We refer to the stronger of these sources as ‘confusing’; they are hard to subtract and the resulting maps are noisier than usual. A few extraneous sources appear within the  $\sim 1'.2 \times 1'.2$  field of view of the 20 cm maps centered on the Seyfert galaxy. These extraneous sources are close enough to the antenna pointing center that they are not bandwidth smeared in the 20 cm maps. They have been deconvolved and mapped and their positions and fluxes are given in the galaxy comments. In this section, radio P.A.’s are listed such that  $0^\circ \leq \text{P.A.} \leq 360^\circ$ .

**Mrk 335 (type 1.0), Fig. 1.** - Our flux is in good agreement with the value of 2.05 mJy at 8.4 GHz obtained by Kukula et al. (1995). There is a confusing source  $\sim 7'$  away. Whittle (1992a) lists the host galaxy as compact and does not list a Hubble T parameter. We have used the NED classification of S0/a for the host galaxy (T=0).

**Mrk 938 (misclassified Seyfert), Fig. 1.** - The 3.6 cm source is extended in P.A.  $125^\circ$ . Gaussian deconvolution of the 20 cm source suggests that it is unresolved, though the contours show a faint extension in a direction consistent with the 3.6 cm extension. The summed flux at 3.6 cm is 7.5 mJy. There is a source (2.5 mJy at 20 cm)  $\sim 1'$  south at position  $\alpha=00^h08^m32^s.69$ ,  $\delta=-12^\circ24'02''.1$  (B1950.0). MWZ claim that this is not a Seyfert galaxy. They find the [OIII] emission weak, while the  $H\alpha$ + [NII] is much stronger over the entire galaxy, implying that the ionization of the gas is not related to any Seyfert activity. The printed edition of RC3 (1991) lists a P.A. of  $30^\circ$  for the galaxy major axis while the updated online version at NED does not list a P.A. ESGC lists a P.A. of  $30^\circ$  and an external diameter of  $2'.19 \times 1'.29$  in B, though this measurement is listed as uncertain. Garnier et al. (1996) measures a major axis P.A. of  $36^\circ$  at an external diameter of  $1'.62 \times 0'.71$  in B.

**NGC 235A (type 1?), Fig. 1.** - A double Gaussian fit to the 20 cm map gives fluxes of 25.5 mJy and 12.5 mJy. The summed flux is 38.5 mJy, consistent with the result of the double Gaussian fit. The NE component is not seen in the 3.6 cm image. There is a confusing source  $\sim 2'$  away. The Seyfert type of this galaxy is uncertain. MWZ, the catalog of Véron-Cetty and Véron (1996) and NED list this galaxy as a Seyfert 1. Keel (1996) and the catalog of Huchra (1989) list it as a Seyfert 2. Maia et al. (1987) have published its

spectrum, and find that it exhibits broad  $H\alpha$  emission. They note that their classification is preliminary because the spectrum was not corrected for underlying stellar absorption, interstellar reddening, and blending of lines. We therefore list this galaxy as a Seyfert 1?, and use a classification of Seyfert 1 for all further analysis. The  $H\alpha+[NII]$  and excitation maps of MWZ show an extension in P.A. similar to the P.A. of the radio extension. RC3 lists a galaxy major axis P.A. of  $117^\circ$  for NGC 235A, and no P.A. for NGC 235B.

**Mrk 348 (type 2), Fig. 2.** - Gaussian deconvolution suggests that the bright core of the source is unresolved in both the 3.6 and 20 cm maps. There appear to be faint extensions to the NNE and SSW at 20 cm. Our measured fluxes of 238 mJy and 302 mJy at 3.6 cm and 20 cm, respectively, are low compared with some previous measurements; earlier observations of this source (Paper V) gave fluxes of 480 and 565 mJy at 6 and 2 cm, respectively. VLBI observations of the source (Neff & de Bruyn 1983) reveal a triple structure in P.A.  $170^\circ$ . The radio source structure is therefore classified as ‘L’. The P.A. of the major axis of the galaxy is not listed in RC3 or UGC. Heckman et al. (1982) mapped the HI in this galaxy and derived P.A.  $\sim 0^\circ$  for the outer HI ring. A deeper HI map (Simpkin et al. 1987) reveals a complex kinematic structure (their Figure 3), in which the kinematic major axis appears to be along P.A.  $170^\circ$ . Falcke et al. (1998) and Capetti et al. (1996) have used high resolution radio and optical images to investigate the detailed correlation of radio structure and ionized gas in this galaxy.

**NGC 424 (type 2), Fig. 2.** The 20 cm map clearly shows an extension in a direction different from the beam extension. The deconvolved source size is less than half the beam size; however the extension, in P.A.  $96^\circ$ , is probably real. The 20 cm map in Paper VII which is at a higher resolution than our 20 cm map, also clearly shows an extension to the E. The central source in the 3.6 cm image is unresolved. The weaker source to the east appeared during the self-calibration process. The P.A. joining the two sources is consistent with the direction of the extension in the 20 cm map. Our 3.6 cm map is similar to the 6 cm map of the same source in Paper VII (where it is listed as TOL 0109-383), in which the weak component to the E is also seen. We classify this source as ‘S’, and adopt a radio P.A. of  $96^\circ$ . Paper VII commented on the flat spectrum of this source -  $\alpha=0.17\pm 0.07$  ( $S_\nu \propto \nu^{-\alpha}$ ) between 6 and 20 cm. Our measured flux of 12.2 mJy at 3.6 cm confirms that the spectrum of the core source is flat to even shorter wavelengths.

**Mrk 565 (misclassified Seyfert), Fig. 2.** The 20 cm emission is diffuse. A Gaussian model fit to the central peak suggests a slight extension in P.A.  $136^\circ$ , in agreement with the



contour map. There is a confusing source  $5.5'$  away and another very strong confusing source  $25'$  away. MWZ find that this is a misclassified Seyfert with very weak [OIII] emission. The 20 cm morphology is similar to that seen in the [OIII] image (MWZ).

**NGC 526A (type 1.9), Fig. 3.** At 20 cm NGC 526A is a triple source. The NW component is itself slightly resolved in P.A.  $113^\circ \pm 5^\circ$ . The distance between the peaks of the SE and NW components is  $17''$ , and the SE component extends another few arcseconds to the SE. Only the central source in NGC 526A is detected at 3.6 cm. NGC 526B, which lies some  $35''$  to the SE of NGC 526A, has also been detected at both 3.6 cm and 20 cm. There is a confusing source  $\sim 3'$  away. The directions of the extensions in the [OIII],  $H\alpha + [NII]$ , and excitation maps of MWZ agree with that of the triple radio source. MWZ, the catalog of Huchra (1989) and Whittle (1992a) list NGC 526A as a Seyfert 2. The catalog of Véron-Cetty and Véron (1996) and NED list it as a Seyfert 1.5. Winkler (1992) discusses the presence of broad  $H\alpha$  and the absence of broad  $H\beta$  in their and other observations of this source. We therefore classify this object as a Seyfert 1.9. The P.A. of the major axis of NGC 526 is listed in RC3 as  $112^\circ$  which is the P.A. between NGC 526A and NGC 526B. We have measured a major axis P.A. of  $60^\circ$  for NGC 526A from the outer isophotes of a DSS image.

**NGC 513 (type 2), Fig. 3.** This galaxy was not observed at 3.6 cm. The extended emission in the 20 cm map has a maximum extent of  $32''$  in P.A.  $\simeq 58^\circ$ . A Gaussian deconvolution of the central source indicates an extent of  $1.1''$  in P.A.  $167^\circ$ . We use this value for the radio P.A. as we are interested in the nuclear structure rather than the diffuse extended emission. The morphology of the 20 cm extended emission is similar to that seen in the [OIII] and  $H\alpha + [NII]$  images (MWZ). All these images align well with the galaxy disk suggesting an origin related to stellar processes rather than the nuclear activity. The morphological type is listed as .S?... in RC3, so we do not list a T parameter value for this galaxy in Table 1.

**Mrk 359 (type 1.5), Fig. 3.** The 20 cm nuclear source sits on a plateau of faint, possibly real emission. Gaussian deconvolution suggests the nuclear source is extended in P.A.  $\simeq 69^\circ$ , but the source size is less than half the beam size. Gaussian deconvolution of the 3.6 cm source suggests that it is unresolved; however, the contours show a faint extension in P.A.  $\sim 80^\circ$ , more or less consistent with the P.A. in the 20 cm map. We therefore list the source as '(S)' and adopt an overall radio P.A. of  $75^\circ$ . There is a strong (800 mJy at 20 cm) double-lobed confusing source - IC 0115 - some  $10'$  away which is difficult to clean

out. Mrk 359 is a narrow line Seyfert 1 (Veilleux 1991).

**Mrk 1157 (type 2), Fig. 4.** The position of the 20 cm peak is listed in Table 1 and the elongated 20 cm source includes both the 3.6 cm components. The NW component is slightly resolved at 3.6 cm in P.A.  $153^\circ$ . The 20 cm flux measured here agrees with an earlier measurement of 24.5 mJy (Paper VII). Combination of the present 3.6 cm fluxes with those at 6 cm reported in Paper VII gives spectral indices of  $\simeq 0.9$  and  $0.7$  for the NW and SE components, respectively. The axis of the radio double is well aligned with the extension in the [OIII] image of MWZ; higher resolution optical maps are required for a detailed comparison.

**Mrk 573 (type 2), Fig. 4.** The 3.6 cm map shows both 20 cm components and a third close to the optical nucleus. The NW and SE components are in P.A.  $309^\circ$  and  $120^\circ$  relative to the central source, respectively. An overall radio P.A. of  $125^\circ$  is adopted, in excellent agreement with earlier maps (Paper V; Kukula et al. 1995; Falcke et al. 1998). Our measured fluxes at 3.6 cm are similar to previously measured 3.6 cm fluxes of 0.78, 0.63 and 0.53 mJy for the NW, central and SE components, respectively (Kukula et al. 1995). Falcke et al. (1998) use higher resolution and sensitivity radio and HST images to investigate the detailed correlations between the radio structure and the ionized gas in this galaxy (see also Capetti et al. 1996). There is a confusing source  $\sim 9'$  away. The P.A. of the major axis of the host galaxy has not been listed in the RC3 or UGC catalogs, as both catalogs find the galaxy to be almost circular. We have confirmed this using a deeper second generation DSS image.

**Mrk 577 (misclassified Seyfert).** This galaxy has not been detected at either 3.6 cm or 20 cm. There is a confusing double source  $\sim 7'$  away. The [OIII] emission is very weak in this galaxy (MWZ), so that the radio non-detection is not unexpected.

**NGC 788 (type 2), Fig. 4.** A Gaussian fit to the 20 cm source indicates an extension in P.A.  $62^\circ$ . Since the deconvolved source size is half the beam size we classify this source as '(S)'. Paper VII has measured fluxes of 2.2 mJy and 1.2 mJy at 20 cm and 6 cm, respectively. There is a double source (17.6 mJy at 20 cm)  $\sim 80''$  from the pointing center, at  $\alpha=01^h58^m39^s.67$ ,  $\delta=-07^\circ04'30''.8$  (B1950.0) and a confusing source  $\sim 8'$  away. The P.A. of the major axis of the host galaxy is not given in RC3 (which lists  $\log R_{25} = 0.12$ ). ESGC lists a major axis P.A. of  $75^\circ$  at an external diameter of  $4'.07 \times 2'.57$  in B. We measure a major axis P.A. of  $125^\circ$ , at an extent of  $4'.1 \times 3'.3$ , from a DSS image.

**ESO417-G6 (type 2), Fig. 5.** A Gaussian fit to the 20 cm source suggests a P.A. of  $6^\circ$ . The closer inspection of the contour map shows that while the extension starts at this P.A. the lower contours to the south show a P.A. closer to  $170^\circ$ . The reality of the northern source in the 3.6 cm map is doubtful, but it is consistent with the N-S elongation seen at 20 cm. We adopt a radio classification of ‘S’ and an overall radio P.A. of  $0^\circ$ . There is a strong confusing source  $\sim 11.5'$  away. ESO lists the galaxy major axis P.A. as  $130^\circ$  but considers it uncertain. RC3 also lists this P.A. as  $130^\circ$ . DSS images show that this P.A. is probably affected by a companion object; the galaxy itself is quite circular.

**Mrk 1066 (type 2), Fig. 5.** A single Gaussian model fit to the 20 cm source indicates a P.A. of  $137^\circ$ . In the 3.6 cm image, the central source has a flux of 4.8 mJy. The NW extension is at P.A.  $\simeq 305^\circ$  w.r.t. the core and has a summed flux of 5.1 mJy. The SE extension is at P.A.  $\simeq 140^\circ$  w.r.t. to the core; its summed flux of 6.5 mJy is less certain as the emission is more diffuse. We adopt a P.A. of  $130^\circ$  for the 3.6 cm image. Our 20 cm flux agrees with the measurement of 94.3 mJy in Paper VII. The axis of the radio source is similar to that of the [OIII] emission and the extent of the radio emission is similar to the extent of the brighter parts of the [OIII] image. Bower et al. (1995) have used the same 3.6 cm radio data in a detailed comparison with HST emission-line images and ground-based optical spectroscopic data.

**Mrk 607 (type 2), Fig. 5.** The extension of the lowest contour in the 3.6 cm map is probably noise. The N-S extension in the 20 cm map is also probably not real. There are three confusing sources, the closest being  $500''$  away.

**Mrk 612 (type 2), Fig. 6.** The northern source in the 20 cm map is extended in P.A.  $\simeq 10^\circ$  and the peak to peak P.A. of the two components is  $170^\circ$ . The 3.6 cm image consists of a knot close to the optical nucleus, emission to the north elongated perpendicular to the source axis, suggestive of a transverse shock, and faint emission to the S. The peak to peak P.A. of the two strongest components in the 3.6 cm image is  $10^\circ$ , in agreement with the extension of the northern component at 20 cm. The southern component of the 20 cm image is seen very faintly in the 3.6 cm map as a few weak knots with a total flux between 0.2 and 0.7 mJy. The overall radio P.A. of the object is taken as  $10^\circ$ . There is a confusing source  $\sim 9'$  away. The P.A. of the major axis of the host galaxy is listed in the printed edition of RC3 (1991) as  $95^\circ$  but is not listed in the updated online version available at NED. A second generation DSS image shows that the outer isophotes of the galaxy are ill-defined.

**NGC 1358 (type 2), Fig. 6.** A Gaussian deconvolution of the 20 cm source suggests a small extension in P.A. between  $116^\circ$  and  $138^\circ$ , consistent with the extension seen in the lower contours. It is not certain if the faint extension seen in the 3.6 cm map is real. We classify the source as ‘(S)’ with a 20 cm (and overall radio) P.A. of  $120^\circ$ . Paper VII measured a 20 cm flux of 3.8 mJy (in agreement with the present flux) and a 6 cm flux of 1.2 mJy. There is a weak confusing source  $6'$  away and a stronger confusing source  $13.5'$  away, both of which do not clean out very well. ESGC lists galaxy major axis P.A. =  $165^\circ$  at an external diameter of  $4.07 \times 3.08$  in B. The printed edition of RC3 (1991) lists major axis P.A. =  $165^\circ$  and  $\log R_{25} = 0.1$ . However the updated online version of RC3 (available at NED) does not list a P.A. Second generation DSS images show that the galaxy is very close to circular.

**NGC 1386 (type 2), Fig. 6.** There is a clear extension in the lower contours of the 3.6 cm map in P.A.  $\sim 170^\circ$ . This extension is present before the self-calibration process and remains after multiple iterations with self-calibration. The source is therefore listed as ‘S’ with P.A.  $\simeq 170^\circ$ . This value is different from the P.A. of  $-125^\circ$  reported in Paper VI from a 6 cm map; we believe the present 3.6 cm map is more reliable. There is a strong confusing source  $\sim 16'$  away. The 20 cm flux of 28.8 mJy measured here is marginally higher than the value of  $23.0 \pm 2.0$  mJy published in Paper VI.

**ESO362-G8 (type 2), Fig. 7.** Gaussian deconvolution of the 20 cm source suggests that it is unresolved. The 3.6 cm map is noisy but shows a faint extension  $\simeq 2''$  to the north. The detached component  $3''$  N of the peak in the 3.6 cm map may not be real. The P.A. between the two peaks separated by  $1''$  in the 3.6 cm map is  $170^\circ$ , but since there is significant emission to the west of the northern peak we adopt a 3.6 cm P.A. of  $165^\circ$ . There are two confusing sources at  $3'$  and  $\sim 9'$ , and another weak source  $2.5'$  away. The radio extension is in a similar direction to the extension seen on a similar spatial scale in the [OIII] and excitation maps of MWZ.

**ESO362-G18 (type 1.5), Fig. 7.** A Gaussian fit to the 20 cm source indicates a deconvolved size of about half the beam size and a P.A. in the direction of the beam; this apparent extension is probably not real. There is a double-lobed confusing source  $\sim 5'$  away.

**NGC 2110 (type 2), Fig. 7.** A single component Gaussian fit to the 20 cm source indicates a P.A. of  $9^\circ$ . The P.A. of the ridge line of the 3.6 cm jets is also  $9^\circ$ . A Gaussian deconvolution of the central peak in the 3.6 cm map gives a flux of 77.6 mJy. The total

summed flux in the central peak is 81.2 mJy (the difference of 3.6 mJy is probably due to the small eastern extension). Radio maps of this source have been previously published by Ulvestad & Wilson (1983) and in Paper VI.  $H\alpha$ + $[NII]$  and  $[OIII]$  images have been published by Mulchaey et al. (1994) and Wilson, Baldwin & Ulvestad (1985) and the relationship between the radio and emission-line structures has been discussed by Mulchaey et al. (1994). The P.A. of the major axis of the host galaxy is not listed in the RC3 or UGC catalogs. ESGC lists a major axis P.A. of  $20^\circ$  at an external diameter of  $2'.45 \times 1'.86$  in B. Wilson & Baldwin (1985) find that the kinematic axis of the inner  $\sim 10''$  of the galaxy is  $161^\circ \pm 2^\circ$  while the photometric axis of the inner  $\sim 30''$  of the galaxy is  $163^\circ \pm 3^\circ$ .

**Mrk 3 (type 2), Fig. 8.** The 3.6 cm map shows a triple structure in a direction consistent with the extension in the 20 cm map. The 3.6 cm flux of the central component (listed as ‘E1’ in Table 2) has been measured by both Gaussian deconvolution and flux summation and found to be  $7.5 \pm 1$  mJy. The images are similar to those published in Paper V; higher resolution maps are given by Kukula et al. (1993). Capetti et al. (1996) provide a detailed discussion of the correlation of radio and emission-line structure in this galaxy. RC3 lists a  $\log R_{25}$  of 0.06 and does not list a major axis P.A. Thompson & Martin (1988) used enlarged Sky Survey prints to measure a major axis P.A. of  $15^\circ$  for the brighter isophotes. A DSS image shows that the outer isophotes of this galaxy are close to circular.

**Mrk 620 (type 2), Fig. 8.** After Gaussian deconvolution, the core of the 20 cm map is elongated  $\simeq 1''.1$  FWHM in P.A.  $95^\circ$ , which agrees with the axis of the double source seen at 3.6 cm. The 20 cm contours to the NE suggest a larger scale extension in P.A.  $\simeq 40^\circ$ , similar to the elongation of the  $H\alpha$ + $[NII]$  image of MWZ.

**Mrk 6 (type 1.5), Fig. 8.** The central source in the 20 cm map is extended in P.A.  $177^\circ$ , in agreement with the P.A. found in Paper V. The larger scale structure in the 20 cm map (listed as ‘Ext’ in Table 2) has P.A.  $\simeq 75^\circ$ , in agreement with the P.A.  $\simeq 87^\circ$  observed by Baum et al. (1993). At 3.6 cm, the source is a triple with a roughly N-S axis. The weak southernmost extension is labelled SW in Table 2. Higher resolution radio maps are published in Kukula et al. (1996).

**Mrk 10 (type 1.2), Fig. 9.** This galaxy was observed at only 20 cm. There is a 9 mJy double source in the same field at  $\alpha=07^h43^m15^s.31$ ,  $\delta=61^\circ04'52''.9$  (B1950). There is also a strong confusing source  $4'.5$  away.

**Mrk 622 (type 2), Fig. 9.** The 20 cm map has large noise stripes running across it due to confusing sources. Gaussian deconvolution of the 20 cm source suggests an extension in P.A.  $0^\circ$ . There are two nearby confusing sources  $\sim 2.2$  and  $2.5$  away. Garnier et al. (1996) measure an external diameter of  $0.81 \times 0.35$  in B and a galaxy major axis P.A. of  $91^\circ$ , while RC3 lists  $\log R_{25} = 0.03$  and does not list a major axis P.A. A first generation DSS image confirms that the galaxy is nearly circular.

**MCG–5-23-16 (type 2).** Paper VI lists this source as ‘S’ with an extent of 75 pc but does not list the P.A. of the extension, or publish a map of the source.

**Mrk 1239 (type 1.5).** Radio maps of this source have been published in Ulvestad et al. (1995). The host galaxy type is listed as ‘E-S0’ in NED, while Whittle (1992a) lists the host galaxy type as ‘compact’.

**NGC 3081 (type 2), Fig. 9.** The 20 cm map shows an extension to the NW and a Gaussian model fit indicates a P.A. of  $158^\circ$ . However, the deconvolved source size is smaller than the beam size and the map has noise stripes along P.A.  $\sim 158^\circ$ . Gaussian deconvolution of the 3.6 cm source suggests a P.A. of  $170^\circ$ , roughly consistent with the P.A. in the 20 cm image. Like the 20 cm map, the 3.6 cm map has noise stripes along P.A.  $\sim 158^\circ$  and the deconvolved source size is slightly smaller than the beam size. Since the 3.6 and 20 cm sources display a consistent P.A. of extension we list this source as ‘(S)’. The 20 cm flux of 3.5 mJy is higher than the value of 2.5 mJy given in Paper VII. There is a confusing source  $\sim 10'$  away, and a very strong confusing source more than  $20'$  away. These do not clean out well and contribute noise to the final maps. The optical morphology of the host galaxy is known to be complex (Storchi-Bergmann et al. 1996). The major axis P.A. is listed as  $158^\circ$  in the ESO catalog, but this determination is listed as uncertain. RC3 also lists a P.A. of  $158^\circ$ , while the ESO Surface Photometry Catalog lists a P.A. of  $74^\circ$ . Buta & Purcell (1998) have measured a photometric galaxy major axis P.A. of  $71^\circ$ , a photometric inclination of  $34^\circ$ , a kinematic major axis P.A. of  $97^\circ$  and a kinematic inclination of  $39\text{--}48^\circ$ . They argue that the kinematic major axis P.A. and the photometric inclination are more reliable. Pogge (1989) has published  $H\alpha + [\text{NII}]$  and  $[\text{OIII}]$  images of this object.

**MCG–2-27-9 (type 2).** An error caused the pointing center to be off by  $\sim 85''$  so we do not publish these maps. Colbert et al. (1996) have published a lower resolution radio map of this source.

**NGC 3516 (type 1.2), Fig. 10.** The 20 cm map shows an extension to the north in P.A.  $\sim 8^\circ$ , but the 3.6 cm map shows only the unresolved nucleus. There is a strong confusing source  $\sim 4'$  away which is very difficult to clean out. Miyaji, Wilson & Pérez-Fournon (1992) present deeper radio images of this source which reveal a P.A. of  $10^\circ$  for the central source and a larger scale northern extension, the P.A. of which increases from  $10^\circ$  to  $20^\circ$  with increasing distance from the nucleus. We measure a radio extent of  $0''.65$  (0.17 kpc) in our 20 cm map but use an extent of 4 kpc from Miyaji et al. (1992). Miyaji et al. (1992) measured fluxes at 20 cm of 4.31 and 2.17 mJy for the N and S components of the central source, respectively. We do not completely resolve these two components but our total flux of 9.4 mJy is significantly higher than the sum of Miyaji et al.'s (1992) fluxes. UGC lists a host galaxy major axis P.A. of  $55^\circ$ , a blue size of  $2'.1 \times 1'.8$  and a red size of  $2'.3 \times 2'.0$ . However, RC3 does not list a P.A. for the major axis. Thompson & Martin (1988) used enlarged Sky Survey prints to derive a P.A. of  $55^\circ$  for the brighter isophotes, but list this as an unsure determination. We used a POSS-E Red plate from DSS to measure a P.A. of  $55^\circ$ . Arribas et al. (1997) find the stellar-kinematic line of nodes to be  $53^\circ \pm 5^\circ$  over the inner  $\sim 10''$  of the galaxy. Since the kinematic and photometric axes are in close agreement we use a major axis P.A. of  $55^\circ$  with a quality flag of ‘a’. Ho et al. (1997) use the criterion of Whittle (1992a) to classify this object as a Seyfert 1.2, which agrees with the classification in Whittle (1992a).

**NGC 4074 (type 2), Fig. 10.** A Gaussian deconvolution of the 20 cm source suggests that it is unresolved, but the contours appear to have an extension in P.A.  $\approx -45^\circ$ . The source is weak at 3.6 cm but a Gaussian deconvolution suggests an elongation in P.A.  $131^\circ$ . The extension in the 3.6 cm source appears in both uniformly and naturally weighted maps and is in the same direction as the extension seen in the 20 cm map. We therefore list this source as ‘S’, with a radio P.A. of  $131^\circ$ . There is a confusing source  $\sim 6'.7$  away. This galaxy is not listed in RC3, UGC or ESO. We used second generation DSS images to measure a major axis P.A. of  $127^\circ$  at an extent of  $1'.1 \times 0'.9$ .

**NGC 4117 (type 2), Fig. 10.** There is a large confusing ‘stripe’ on the 20 cm map but no confusing source could be found within a radius of a degree. The maps are therefore noisy. The source is quite weak and the structure would normally be considered unreliable, but the 20 cm map of Paper VII shows a similar N-S extension. We therefore classify the radio morphology as ‘(L)’ at 20 cm in P.A.  $177^\circ$ . The galaxy is not detected at 3.6 cm. Paper VII lists a 20 cm flux of 2.8 mJy for this object, which is marginally higher than the present value, and a flux upper limit of 0.6 mJy at 6 cm, so that our non-detection at 3.6 cm is not surprising.

**NGC 4253 (type 1.5), Fig. 11.** The 20 cm source appears more circular than the beam and a Gaussian deconvolution indicates a P.A. of  $169^\circ$ . However, this P.A. is in the direction of a sidelobe pattern and the source size is only 1.1 times the beam size, so the reality of the apparent extent is suspect. The lower contours on the 3.6 cm source exhibit extensions both in P.A.  $\sim 160^\circ$  (in agreement with the direction of the possible extension at 20 cm) and P.A.  $\sim 55^\circ$ . A Gaussian deconvolution indicates an extension in P.A.  $32^\circ$  for the brighter isophotes. This source has also been observed with the VLA in ‘A configuration’ at 3.6 and 6 cm by Ulvestad et al. (1995). They find the source to have an extension in P.A.  $22^\circ \pm 4^\circ$  at 3.6 cm (with a weaker extension in P.A.  $-30^\circ$ ) and in P.A.  $12^\circ \pm 5^\circ$  at 6 cm. Ulvestad & Wilson (Paper V) observed this source at 6 cm and derived a P.A. of  $16^\circ$ . Kukula et al. (1995) observed this source at 3.6 cm with similar resolution to ours and find an extension in P.A.  $27^\circ$ . The source therefore appears to be extended in both P.A.  $\sim 27^\circ$  (on a scale of  $0''.25$ ) and P.A.  $160^\circ$  (on a scale of  $0''.3$ ). We classify this source as ‘S’, and adopt radio P.A.  $\simeq 27^\circ$  as representative of the source axis on the smallest scales. The 20 cm flux measured here is consistent with the value of 36.4 mJy published in Paper VII. UGC gives a host galaxy diameter of  $0'.89 \times 0'.89$  in B and  $0'.89 \times 0'.79$  in R. Takase et al. (1987) find a galaxy diameter of  $0'.9 \times 0'.7$ . MacKenty (1990) finds the galaxy to have a major axis P.A. of  $69^\circ$  (at a major axis extent of  $41''$ ), and a minor to major axis ratio (b/a) of 0.89. We used second generation DSS images to measure a P.A. of  $60^\circ$  at an extent of  $1'.3 \times 1'.15$ .

**ESO323-G77 (type 1.2), Fig. 11.** Both the 20 cm and 3.6 cm maps of this southern source are noisy. The 20 cm source is extended in P.A.  $24^\circ \pm 15^\circ$ , in agreement with the extension at 3.6 cm. A naturally weighted image at 3.6 cm shows a double source in P.A.  $\simeq 40^\circ$ . There is a confusing source  $\sim 3'.7$  away.

**NGC 5077 (misclassified Seyfert; Liner type 1.9), Fig. 12.** Gaussian deconvolution shows that the galaxy is unresolved at both 3.6 and 20 cm. The source has a flat spectrum between 3.6 and 20 cm. Previous high resolution VLA observations of this source (Wrobel & Heeschen 1984) give fluxes of 109, 90 and 111 mJy at 1.5, 4.9 and 15 GHz, respectively; the source was unresolved in high resolution maps at all three frequencies. The large scale features in the 20 cm self-calibrated map were not seen by Wrobel & Heeschen (1984) but may be real considering the morphology of the extended emission seen in the [OIII] and  $H\alpha + [\text{NII}]$  images of MWZ.



**MCG–6–30–15 (type 1.2), Fig. 12.** The source is unresolved at both 3.6 and 20 cm. There is another source (76 mJy at 20 cm) at  $\alpha=13^h33^m06^s.07$ ,  $\delta=-34^\circ04'49''.0$  (B1950.0). The position listed in Table 1 is that of the peak at 3.6 cm. The 20 cm source position is offset by  $\sim 1''.4$  to the SE and is at  $\alpha=13^h33^m01^s.93$ ,  $\delta=-34^\circ02'26''.6$  (B1950.0), but is consistent with the 3.6 cm position given the weakness of the source. The 20 cm flux measured here is more than twice the value of  $1.7\pm0.7$  mJy published in Paper VI.

**NGC 5252 (type 1.9), Fig. 12.** Gaussian deconvolution of the nuclear (southern) source in the 20 cm map shows it to be extended in P.A.  $170^\circ$ , in close agreement with the P.A. of  $171^\circ$  between the two components. The northern source is unresolved. A Gaussian deconvolution of the core component in the 20 cm map indicates a flux of 12.7 mJy while the summed flux is 13.5 mJy. Our results are consistent with those of Wilson & Tsvetanov (1994) and confirm the relatively flat spectrum of the nucleus ( $\alpha_{3.6}^{20} = 0.32$ ). The extent of the S (nuclear) component in the 20 cm map is 0.65 kpc. Wilson & Tsvetanov (1994) suggest the N component is associated with NGC 5252 rather than being an unrelated background source. We therefore adopt a radio extent of 14.79 kpc which is the distance between the two components. Emission line fluxes for the S (nuclear) component have been taken from Acosta-Pulido et al. (1996), who also list earlier determinations of the flux. Acosta-Pulido et al. (1996) find evidence for a nuclear broad  $H\alpha$  line, but no broad  $H\beta$  line, which leads to a classification of Seyfert 1.9 for this object.

**Mrk 270 (type 2), Fig. 13.** The 20 cm map shows two components. At 3.6 cm, both components are detected in a natural weighted (robust=4) map. The NE source is weakly detected in a uniformly weighted (robust=0) map. Our maps are in agreement with those of Paper V. The P.A. and separation of the radio double agree well with the major axis P.A. and extent of the brighter [OIII] and  $H\alpha$ + [NII] extension (MWZ); higher resolution optical images are required for a detailed comparison. The P.A. of the host galaxy is not listed in RC3. UGC lists the galaxy extent as  $1'.1 \times 1'$  in B and  $1'.1 \times 1'.1$  in R. Second generation DSS images confirm that the galaxy is nearly circular.

**NGC 5273 (type 1.5), Fig. 13.** A Gaussian deconvolution suggests that the 20 cm source is extended in P.A.  $179^\circ$ , but the deconvolved source size is less than half the beam size. The southern extension to the source at 3.6 cm (in P.A.  $\sim 175^\circ$ ) does not appear in a uniformly weighted (robust=-4) map but does appear in the uniformly weighted (robust=0) map and in naturally weighted maps. A Gaussian deconvolution of the 3.6 cm source suggests a P.A. of  $170^\circ$ ; again, the deconvolved source size is less than half the beam size.

Ulvestad & Wilson (Paper VI) have observed this source at 6 and 20 cm and list the source as ‘S’. Their unpublished map shows an extension in P.A.  $5^\circ$ . We therefore adopt a radio source classification of ‘S’ and a radio P.A. of  $5^\circ$ . Paper VII gives a 20 cm flux of 2.5 mJy, in agreement with our measured value, and a 6 cm flux of 0.9 mJy. There is a confusing source  $9\prime.5$  away.  $H\alpha$ + $[NII]$  and  $[OIII]$  images have been published by Pogge (1989). Whittle (1992a) classifies this object as a Seyfert 1.9. Ho et al. (1997) have detected broad lines in both  $H\alpha$  and  $H\beta$ . They have used the criteria of Whittle (1992a) to classify this object as a Seyfert 1.5.

**IC 4329A (type 1.2), Fig. 13.** The extension in P.A.  $\sim 75^\circ$  in the 20 cm map is present before the self-calibration process. Higher resolution 20 cm and 6 cm maps of this source (Unger et al. 1987a) show a diffuse  $6''$  extension in P.A.  $\sim 285^\circ$ . There is another source in the same field (8 mJy at 20 cm) at  $\alpha=13^h46^m25^s.94$ ,  $\delta=-30^\circ02'25''.4$  (B1950.0). The source is suspected to be variable (Unger et al. 1987a). The printed edition of RC3 (1991) lists an erroneous host galaxy P.A. of  $63^\circ$ , while the updated online version (available at NED) lists the correct P.A. of  $45^\circ$ .

**NGC 5548 (type 1.2), Fig. 14.** The northern component seen in the 20 cm map is limb-brightened, while the nuclear component is unresolved (cf. Wilson & Ulvestad 1982). The P.A.’s of the peaks of the northern and southern extensions relative to the core are  $348^\circ$  and  $170^\circ$ , respectively. Neither of the extensions are detected in the 3.6 cm map. There are two other sources in the field, one at  $\alpha=14^h15^m39^s.76$ ,  $\delta=25^\circ21'56''.0$  (B1950.0) and a double source at  $\alpha=14^h15^m35^s.82$ ,  $\delta=25^\circ22'08''.3$  (B1950.0). There is also a confusing source  $\sim 4'$  away. The radio sources in the field around NGC 5548 are discussed in detail by Wilson & Ulvestad (1982). The flux ratio  $R = F_{[OIII]} / F_{H\beta}$  listed by Whittle (1992a) leads to a classification of Seyfert 1.2 while Ho et al. (1997) use the criterion of Whittle (1992a) to classify this object as a Seyfert 1.5. We use a classification of Seyfert 1.2 as long term monitoring of the BLR in NGC 5548 (Peterson et al. 1991) consistently gives  $R \lesssim 0.75$ . UGC lists a major axis P.A. of  $110^\circ$  at an extent of  $1\prime.7 \times 1\prime.5$ . The optical morphology of this galaxy is, however, complex, and we do not list a major axis P.A. for it.

**NGC 6251 (type 2), Fig. 14.** The jet of this famous radio galaxy (see e.g. Perley, Bridle & Willis 1984) is not detected in the 3.6 cm map. The jet extends well beyond the synthesized field of view of our 20 cm map and we detect only the innermost part of it. For this reason, the total 20 cm flux listed in Table 1, and the 20 cm flux of the jet listed in Table 2, are underestimates of the actual fluxes.

**NGC 7465 (type 2), Fig. 15.** In the 20 cm map, the source sits on a large, low level plateau so the flux value is uncertain. Gaussian deconvolution of the 3.6 cm source suggests a P.A. of  $32^\circ$ , but the source size is less than half the beam size. There is a significant displacement ( $3''$ ) between the apparent positions of the 3.6 cm and 20 cm sources. The VLA calibrator manual lists a position code of ‘Terrible’ (‘positional error  $> 0''.15$ , and frequently much greater’) for 2247+140, the calibrator used at 20 cm. Since the 3.6 cm calibrator, 2251+158, has a position code of ‘A’ (positional error  $< 0''.002$ ) and the 3.6 cm resolution is higher than the 20 cm resolution, the position of the 3.6 cm source is more reliable and is listed in Table 1. The position angle of the major axis of the host galaxy is not listed in the RC3 or UGC catalogs. UGC lists an external diameter of  $1.2 \times 0.7$  in B. A second generation DSS image reveals a diameter of  $\sim 1.7$  but shows clear signs of interaction between NGC 7465 and two nearby galaxies.

## 5. Statistical Results

In this section, we perform a statistical study of the radio properties of Seyfert galaxies. We include only the 43 galaxies in the early-type Seyfert sample (Section 2), except for Section 5.4, where the sample is expanded to include other Seyfert galaxies.

To test for correlations in our data, we use the techniques of “survival analysis” as coded in the ASURV software package (Lavalley, Isobe & Feigelson 1992). We use the 5 available univariate tests - Gehan’s generalized Wilcoxon test with permutation variance, Gehan’s generalized Wilcoxon test with hypergeometric variance, the logrank test, the Peto-Peto test and the Peto-Prentice test - to estimate the probability that two distributions are not derived from the same parent population. Note that for completely “uncensored” data, i.e. data which contains no upper or lower limits, the Peto-Peto test reduces to the logrank test and the Peto-Prentice method reduces to Gehan’s Wilcoxon test. We use the 3 available bivariate tests - Cox proportional hazard model, generalized Kendall’s  $\tau$ , and Spearman’s  $\rho$  - to test for correlations between two variables within a sample. The result of each bivariate test is a value which represents the probability that the two variables are not correlated. We consider a result to be statistically significant only if all relevant ASURV statistical test results are less than 0.05 and “weakly” significant if all relevant ASURV test results are less than 0.10, or if all except one test result are less than 0.05. We use the Kaplan-Meier estimator, also from the ASURV package, to calculate the mean of a distribution which contains censored (upper or lower limit) data points. The numerical results of the statistical tests are listed in Table 6 (univariate tests) and Table 7 (bivariate tests).

All P.A. measurements are subject to uncertainty. In an attempt to keep track of these uncertainties, we have provided quality flags, as outlined in Section 3 and Table 4 to each radio P.A. and host galaxy P.A. determination. The color coding used in the following histograms reflects this quality control - dark shades are used for more reliable data and lighter shades for less reliable data. The P.A.'s of the [OIII], H $\alpha$  and green emission from MWZ have also been color coded according to data quality, and this coding is explained in the relevant figure captions. Because of the small number of objects in our sample, data quality flags have been ignored when doing statistical tests (Tables 6 and 7).

### 5.1. Sample Properties, radio extent and luminosity

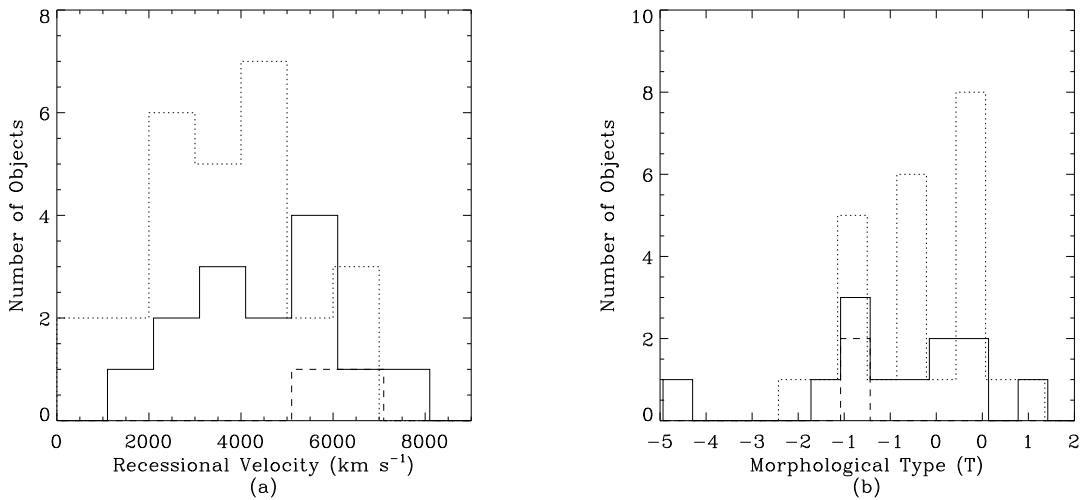


Fig. 16.— Overall properties of the early-type Seyfert sample. Seyfert 1’s (Seyfert 1.0’s through Seyfert 1.5’s) are plotted with solid lines, Seyfert 1.8’s and 1.9’s with dashed lines, and Seyfert 2.0’s with dotted lines. For clarity, the histograms are slightly offset along the x axis. (a) Histogram showing the distributions of recessional velocity; (b) histogram showing the distributions of morphological type.

Some properties of the sample are shown in Figures 16 and 17. The Seyfert 1’s and Seyfert 2.0’s in the early-type radio sample have similar distributions of  $V_{rec}$  and T (Figure 16) though the Seyfert 1’s are marginally more distant. A histogram of 20 cm luminosities (Figure 17a) shows that the 20 cm luminosities of Seyfert 1’s and Seyfert 2.0’s are similar. The distributions of the 3.6 cm luminosities (not shown) give a similar result. The mean 20 cm luminosity ( $P_{20}$ ) of Seyfert 1’s ( $10^{22.72}$  Watts Hz<sup>-1</sup>) and Seyfert 2.0’s ( $10^{22.75}$  Watts Hz<sup>-1</sup>) are not significantly different. The 20 cm radio luminosity of

the sample is uncorrelated with galaxy morphological type (Figure 17b) for both Seyfert types. This is perhaps not surprising given the rather narrow range of morphological types in the sample. As seen in Figure 17c, there is no trend for the fraction of sources with resolved structure to decrease with increasing recessional velocity. The 20 cm luminosity is significantly correlated with radio structural class (i.e. ‘U’, ‘S’ and ‘L’, see Figure 17d) for Seyfert 2.0’s, with the ‘L’s having the largest luminosity, while these two variables are uncorrelated for Seyfert 1’s (Table 7). Consistent with the unified model, Seyfert 2.0’s have a higher fraction of resolved radio sources (25/27 or 93%) than Seyfert 1’s (9/14 or 64%); statistical tests show that this difference is significant (Table 6), but the results are limited by the small number of Seyfert 1’s. The two Seyfert 1.9’s (NGC 5252 and NGC 526A) are ‘L’-class radio sources and are the most radio-extended objects in the sample (Figure 17e). The next three largest radio sources are Seyfert 1.2’s (NGC 3516, IC 4329A and NGC 5548). The existence of these large Seyfert 1’s makes the mean Seyfert 1 radio extent ( $1.2 \text{ kpc} \pm 0.4 \text{ kpc}$ ) greater than the mean Seyfert 2.0 radio extent ( $0.6 \text{ kpc} \pm 0.1 \text{ kpc}$ ) despite the fact that the Seyfert 1’s have a lower fraction of resolved radio sources (the mean sizes were calculated using the Kaplan-Meier estimator, including upper limits). This difference in mean extents is, however, not statistically significant (Table 6). As Figures 17e and 17f suggest, Seyfert 2.0’s show a weak trend for more radio-extended objects to have larger radio luminosities while Seyfert 1’s do not show a correlation between these two quantities (Table 7). We emphasise that studies involving the linear extent of radio sources are limited by ambiguity in the precise definition of this quantity.

## 5.2. The relationship between radio and emission-line gas

The radio and high excitation ionized gas structures in Seyfert 2’s are already known to be highly correlated from VLA and HST images of individual galaxies (e.g. Bower et al. 1994, 1995; Capetti et al. 1996; Falcke et al. 1998). Previous work has shown that the ionized gas radiating emission lines is ionized by photons escaping from the central source (e.g. Wilson and Tsvetanov 1994) and compressed through interactions with the radio ejecta (e.g. Capetti et al. 1996). It is therefore interesting to compare the alignments and the total luminosities of the emission line and radio structures. The distribution of  $\text{P.A.}_{\text{Radio}} - \text{P.A.}_{[\text{OIII}]}$  (Figure 18) for Seyfert 2.0’s shows a strong trend for the two axes to align, while the same distribution for Seyfert 1’s is not significantly different from a uniform distribution (Table 6). The absence of a correlation for Seyfert 1’s is, however, not surprising given that there are only 7 galaxies in the early-type radio sample with a measurement of  $\text{P.A.}_{\text{Radio}} - \text{P.A.}_{[\text{OIII}]}$ . In fact, the distributions of  $\text{P.A.}_{\text{Radio}} - \text{P.A.}_{[\text{OIII}]}$  for Seyfert 1’s and Seyfert 2.0’s are not significantly different from each other (Table 6). The

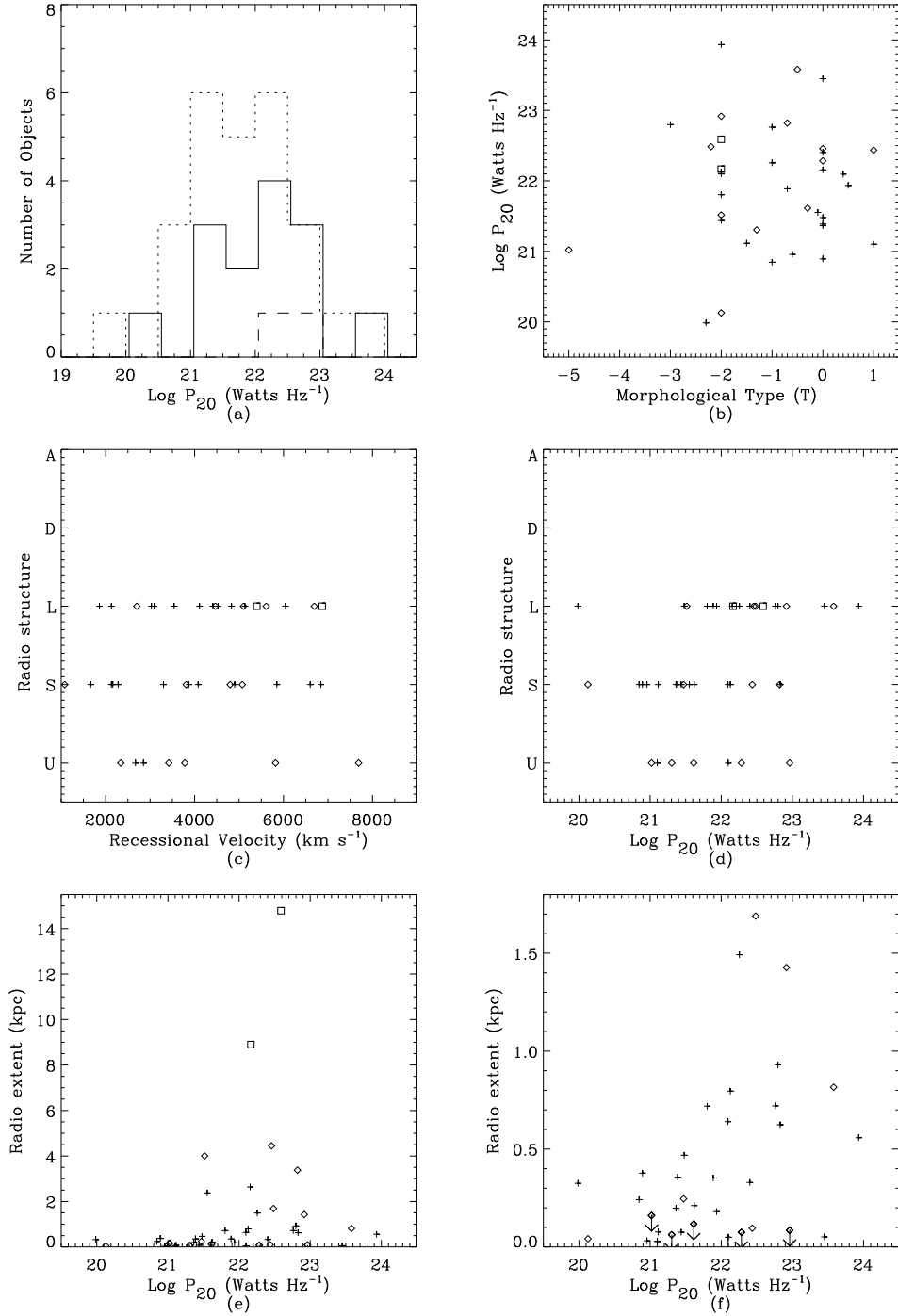


Fig. 17.— Relationships between radio luminosity, structure, extent, galaxy morphological type and recessional velocity for the early-type Seyfert sample. Seyfert 1’s (Seyfert 1.0’s through Seyfert 1.5’s) are plotted with solid lines and diamonds, Seyfert 1.8’s and 1.9’s with dashed lines and squares, and Seyfert 2.0’s with dotted lines and crosses. (a) Histogram showing the distribution of 20 cm radio luminosity. For clarity, the histograms are slightly offset along the x axis; (b) relationship between radio luminosity and galaxy morphological type; (c) relationship between radio structure and recessional velocity. (d) relationship between radio structure and 20 cm radio luminosity; (e) relationship between radio extent and 20 cm radio luminosity. (f) same as (e), but with an enlarged y scale.

distribution of  $P.A._{Radio}-P.A._{H\alpha}$  (Figure 18) for Seyfert 2.0’s also shows a strong tendency for the axes to align while the same distribution for Seyfert 1’s is not significantly different from a uniform distribution (Table 6). Again, there are only 7 galaxies in the distribution for Seyfert 1’s. Previous studies have shown this alignment between radio and emission-line structures for individual galaxies or a small number of galaxies, usually selected to show extended, class ‘L’, radio emission (e.g. Haniff, Wilson & Ward 1988; Whittle et al. 1988). Our result is the first to demonstrate that this alignment is characteristic of early-type Seyfert galaxies *as a class* in a well-defined sample. In our sample, the radio source is smaller than the scale on which the axis of the emission-line gas is measured (by a factor of  $\sim 2 - >5$  for Seyfert 2.0’s), suggesting that the alignment results from the anisotropic escape of ionizing photons preferentially along and around the radio axes, or compression of gas by outflows aligned with the radio source but on a larger scale.

The alignment between the radio and the extended ionized gas also places a strong constraint on any large angle precession of the inner accretion disk, e.g., as theorized to result from radiative instabilities (Pringle 1997) or as inferred from observations in 4C 29.47 (Condon & Mitchell 1984). We consider two cases for the excitation of the ionized gas:

(i) The extended ionized gas is photoionized by a central source and is produced by the intersection of the nuclear ionization cone with the disk of the galaxy. In this case, as demonstrated for NGC 4151 (Pedlar et al. 1993; Boksenberg et al. 1995) and in simulations (Mulchaey et al. 1996b), the position angles of the extended emission-line gas and the ionization cone axis are not necessarily the same. Hence even if the axes of the ionization cone and radio ejecta are exactly aligned, there can be a significant offset ( $30^\circ$  in the case of NGC 4151) between the position angles of the radio structure and the extended ionized gas. We find that the extended ionized gas is preferentially aligned with the disk of the galaxy for the early-type Seyfert 2.0’s (see Section 5.3 and Figure 20), so the scatter of  $\sim 30^\circ$  about  $0^\circ$  in the distribution of  $P.A._{Radio}-P.A._{[OIII]}$  (Figure 18) for Seyfert 2.0’s might be completely explained by such a projection effect. Consider a typical object in the sample with emission-line extent 2 kpc and radio extent 0.5 kpc. The difference between the travel times of the ionizing radiation and the radio ejecta must be significantly less (by at least a factor of 4, if we consider a precession angle  $> 60^\circ$ ). than any precession period,  $P$ , of the collimating disk for the radio and ionization cone axes to be so closely aligned. If the velocity of the radio ejecta in Seyferts is sub-relativistic, as suggested by the proper motion of radio knots in NGC 4151 (Ulvestad et al. 1998) and by the modeling of the interaction between radio ejecta and high-excitation gas in NGC 1068 (Wilson & Ulvestad 1987) and NGC 5929 (Whittle et al. 1986), the crossing time of the ionizing radiation is negligible ( $\sim 10^4$  yr) and we must have  $V_{ejecta} \times P \gtrsim 2$  kpc. Under a number of assumptions, Pringle (1997) calculates that the characteristic precession time of the accretion disk due to the

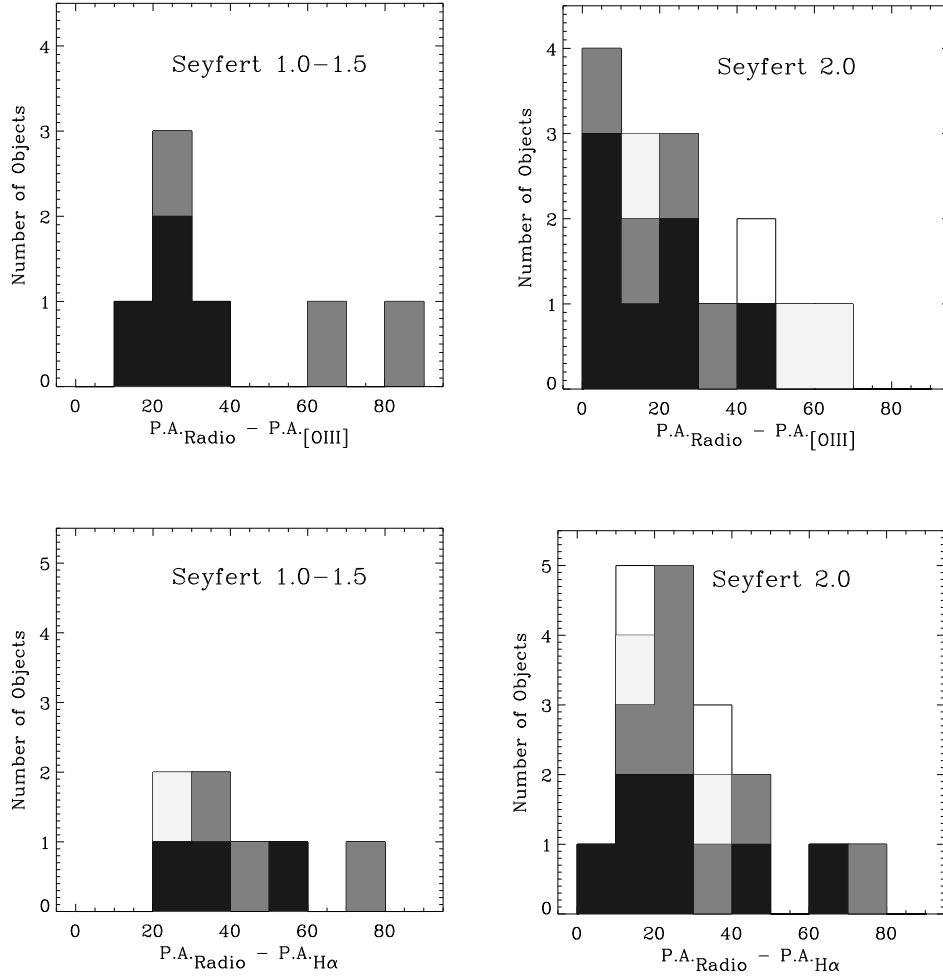


Fig. 18.— Histogram of the difference between the radio and emission-line P.A.’s for the early-type Seyfert sample. Seyfert 1’s (Seyfert 1.0’s through Seyfert 1.5’s) are plotted on the left; Seyfert 2.0’s are plotted on the right. The two Seyfert 1.9’s in the early-type sample are not plotted. Quality flags for  $P.A._{Radio}$  are explained in Table 4. Quality flags for  $P.A._{emission-line}$  are ‘a’, except for values in brackets in Table 3 which are assigned ‘b’. Objects with quality flag ‘a’ for both  $P.A._{Radio}$  and  $P.A._{emission-line}$  are shaded black. Objects with one flag ‘a’ and the other ‘b’ for  $P.A._{Radio}$  and  $P.A._{emission-line}$  are shaded in dark grey. Objects with flag ‘b’ for both  $P.A._{Radio}$  and  $P.A._{emission-line}$  are shaded light grey. All others are in white.

radiative instability is  $t_{var} = 2 \times 10^6 M_8 \alpha^{-1} \text{ yr}$ , where  $M_8$  is the mass of the central black hole in units of  $10^8 M_\odot$  and  $\alpha$  is the usual viscosity parameter. If we use typical values of  $10^8 M_\odot$  for the mass of a Seyfert black hole (e.g. Kormendy & Richstone 1995) and  $\alpha = 1$  then  $V_{ejecta} \gtrsim 1000 \text{ km s}^{-1}$ , which is not unreasonable. Better determinations of the velocity of radio ejecta in Seyferts will provide more stringent constraints on P;

(ii) The extended ionized gas is caused by a large scale, self-ionized outflow (e.g. Bicknell



et al. 1998). The precession period of the collimating disk disk is once more constrained by the difference in the travel times of the radio ejecta and the larger scale outflow. Similar considerations as described above apply, and  $V_{ejecta}$  now refers to the radio ejecta or ionized gas, whichever has the longer crossing time.

The relationships between the radio and emission-line luminosities are shown in Figure 19. At a fixed nuclear radio luminosity, Seyfert 2.0’s appear weaker in [OIII] and  $H\alpha$  as compared to Seyfert 1’s, in agreement with the findings of Whittle (1985). The 20 cm luminosity is uncorrelated with both the [OIII] luminosity and the  $H\alpha$  luminosity for Seyfert 2.0’s (Table 7). For Seyfert 1’s, however, the 20 cm luminosity is significantly correlated with both the [OIII] luminosity and the  $H\alpha$  luminosity (Table 7). These two correlations are significant even after deleting the single Seyfert 1 with low [OIII] and  $H\alpha$  luminosity (ESO 512-G20); in this case the probabilities that the 20 cm luminosity is not correlated with the [OIII] luminosity and  $H\alpha$  luminosity are 0.03–0.06 and 0.015–0.06, respectively. Previous studies with larger samples of Seyferts have found strong correlations between  $L_{[OIII]}$  and  $P_{20}$  (de Bruyn & Wilson 1978; Whittle 1985; Whittle 1992c). The scatter in our plot of  $P_{20}$  vs [OIII], which contains 26 objects (Figure 19a), is similar to that in the plot of [OIII] vs  $P_{20}$  in Whittle (1992c), which contains  $\sim 80$  objects (his Figure 3). It is therefore likely that the reason that our results are not completely consistent with Whittle (1992c) is the smaller number of objects in our sample.

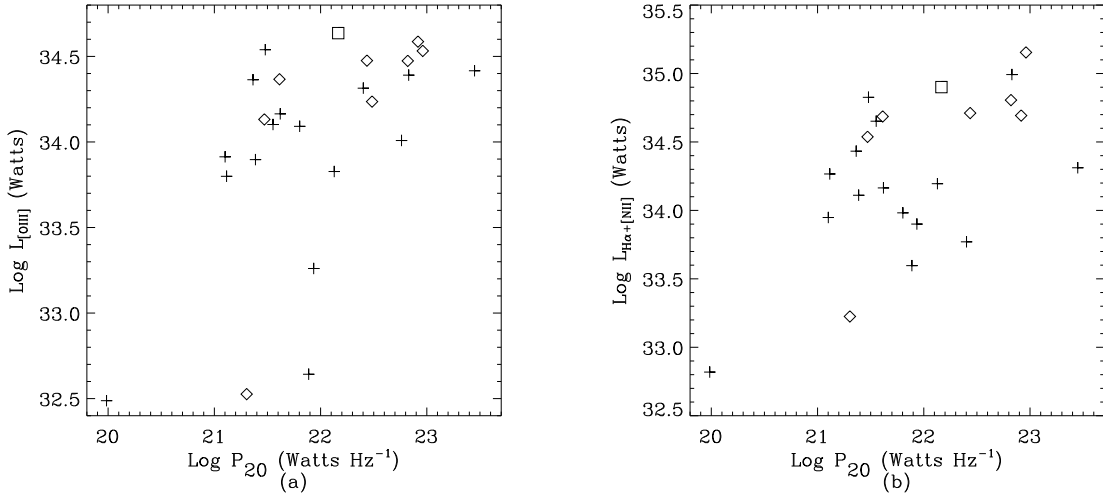


Fig. 19.— Relationships between the luminosities of the [OIII],  $H\alpha$ + [NII] and radio emissions for the early-type Seyfert sample. Seyfert 1’s (Seyfert 1.0’s through Seyfert 1.5’s) are plotted as diamonds, Seyfert 1.8’s and Seyfert 1.9’s as squares, and Seyfert 2.0’s as crosses. (a) Relationship between [OIII] luminosity and 20 cm radio luminosity; (b) relationship between  $H\alpha$ + [NII] luminosity and 20 cm radio luminosity.

### 5.3. The alignment between emission-line structure and host galaxy

The relative orientations of the nuclear [OIII] and nuclear green emission with respect to the major axis of the host galaxy for the early-type Seyfert sample of MWZ have been studied by Mulchaey & Wilson (1995). They measured the “nuclear” orientation of the [OIII] and green emission (on scales of  $3''$ – $4''$ ) and found a close alignment between the [OIII] and green emission, and a weaker alignment between the nuclear [OIII] emission and the host galaxy major axis as listed in the UGC and ESO catalogs.

Here we discuss the relative orientations of the larger scale [OIII] and  $H\alpha$  emission, the larger scale green continuum emission (all from MWZ), and the host galaxy major axis (determined as described in Tables 3 and 4). The P.A.’s of the [OIII],  $H\alpha$  and green emission are listed in Table 3 (for the early-type Seyferts which are extended in the radio) and in Table 4 of MWZ (for the entire early-type Seyfert sample). These P.A.’s have been measured at typical extents of  $5''$ – $10''$ ,  $8''$ – $15''$  and  $20''$ – $40''$  for the [OIII],  $H\alpha$  and green emission, respectively (see Table 4 of MWZ for the exact extents). When determined photometrically, the P.A.’s of the host galaxy major axis were measured at a larger extent (typically  $\geq 2$ ) than the green emission of MWZ. Histograms of the relative orientations are shown in Figure 20. The [OIII] emission is the better tracer of high excitation gas associated with nuclear activity, because  $H\alpha$  is often contaminated by HII regions in the disk of the galaxy. Here, however, the [OIII] and  $H\alpha$  emission tend to be aligned. What is striking about Figure 20 is that, for Seyfert 2.0’s, the [OIII],  $H\alpha$ , green and host galaxy major axes are all significantly aligned with each other (see Table 6). The relationship between these axes is not as clear for Seyfert 1’s, perhaps because of the smaller number of objects. For the Seyfert 2.0’s, the ionized gas tends to align with both the smaller scale radio emission (Figure 18) and the larger scale galaxy disk (Figure 20). This is consistent with a scenario in which ambient gas lying preferentially in the galaxy disk is ionized by an ionization cone from the central engine, and/or compressed by a gaseous outflow, both of which tend to be aligned with the axis of the radio source.

### 5.4. Seyfert radio extents - at odds with the unified scheme ?

Seyfert 2’s show a higher fraction of resolved radio sources as compared to Seyfert 1’s (see Section 5.1 and, e.g., Paper VII). Ulvestad & Wilson (Paper VII) also found a weak trend for Seyfert 2’s to have more extended nuclear radio structures, though we find (Section 5.1) that the existence of a few highly extended Seyfert 1’s in the early-type radio sample makes the mean Seyfert 1 radio extent greater than the mean Seyfert 2.0 radio extent. Within the unified scheme of AGN, which is supported by the fact that Seyfert 1’s

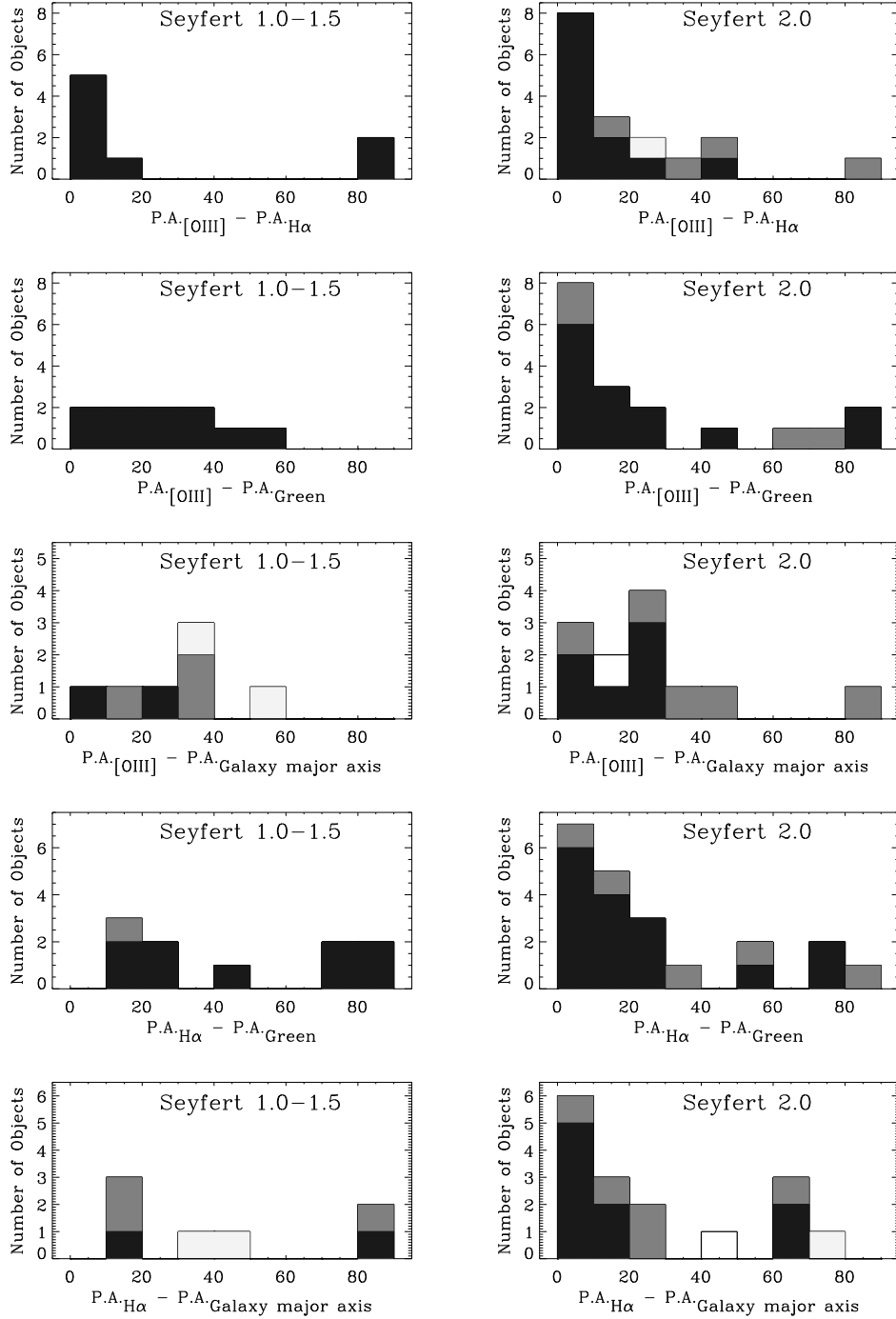


Fig. 20.— Histograms of the differences between the P.A.’s of the [OIII] and  $H\alpha$  structures, the green continuum emission, and the host galaxy major axis as listed in Table 3 and MWZ’s Table 4. The green continuum is measured at a surface brightness of  $2 \times 10^{-18}$  ergs  $s^{-1}$   $cm^{-2}$   $\text{\AA}^{-1}$  (arcsec) $^{-2}$ , which is the lowest contour of the images of MWZ (see Section 3 and Table 3). Quality flags for P.A.*Radio* and P.A.*Galaxy major axis* are explained in Table 4. Quality flags for P.A.*H $\alpha$* , P.A.*[OIII]* and P.A.*Green* are ‘a’, except for values in brackets in Table 3 and MWZ’s Table 4 which are assigned ‘b’. Objects with quality flag ‘a’ for both P.A. values are shaded black. Objects with one flag ‘a’ and the other ‘b’ for the two P.A. values are shaded in dark grey. Objects with flag ‘b’ for both P.A. values are shaded light grey. All others are in white.

and 2’s have similar radio luminosities, we would expect the radio extent to be correlated with Seyfert type, with Seyfert 1.0’s having the lowest and Seyfert 2.0’s having the highest mean projected radio extent.

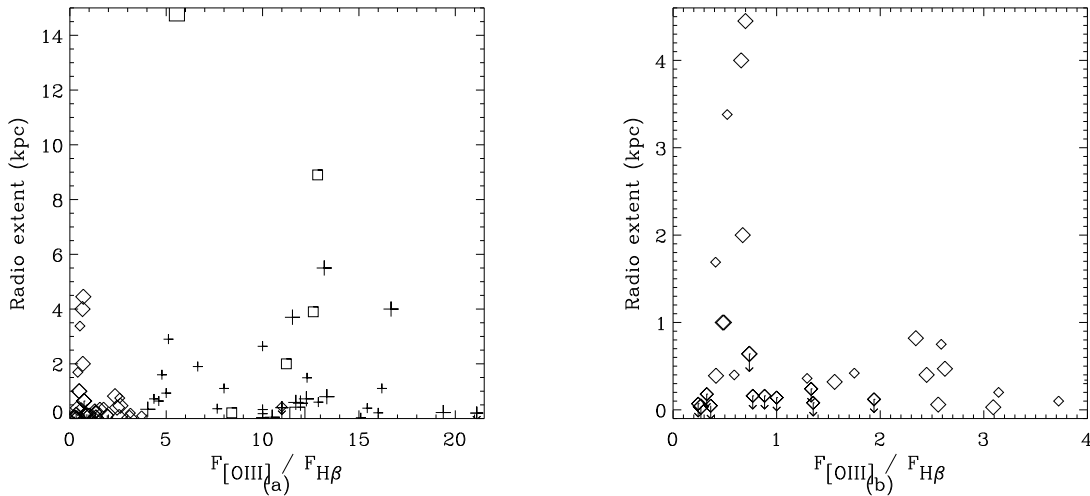


Fig. 21.— The relationship between Seyfert radio extent and  $R=F_{[OIII]}/F_{H\beta}$  for an enlarged sample of Seyfert galaxies (see Section 5.4). Seyfert 1’s (Seyfert 1.0’s through Seyfert 1.5’s) are plotted as diamonds; Seyfert 2.0’s are plotted as crosses; Seyfert 1.8’s and Seyfert 1.9’s are plotted as squares. Large symbols denote higher quality data, for which the radio extent, [OIII] flux and  $H\beta$  flux have at least one quality flag ‘a’, and the others ‘b’ or higher. Fluxes from Winkler (1992) have been assigned quality flag ‘b’. Smaller symbols are used for the lower quality data. (a) Relationship between radio extent and  $R$ ; (b) same as (a), but with a smaller x and y axis range.

We therefore investigate the relationship between radio extent and  $R=F_{[OIII]}/F_{H\beta}$ . The parameter  $R$  is used (see e.g. Veilleux & Osterbrock 1987) both to distinguish Seyfert 2’s from other emission-line nuclei (such as LINERs and HII regions), and to distinguish the sub-classes 1.0, 1.2, 1.5 and 1.8 among Seyfert 1’s (see Section 3). Since the early-type Seyfert sample is too small for this investigation, we have added to it all Seyferts from the literature which show extended radio structure (see Nagar & Wilson 1998 for a list of these objects), and all radio-unresolved Seyferts from Papers V, VI, VII, and Kukula et al. (1995), for which values of [OIII] flux and  $H\beta$  flux are listed in Whittle (1992a) and Winkler (1992). The final sample includes 21 radio-extended Seyfert 1’s, 11 radio-unresolved Seyfert 1’s, 6 radio-extended Seyfert 1.8’s and 1.9’s, 27 radio-extended Seyfert 2.0’s and 4 radio-unresolved Seyfert 2.0’s. The results are shown in Figure 21.

It is remarkable that all 5 highly extended Seyfert 1’s (extent  $\geq 1.5$  kpc) have  $R$  values in a relatively narrow range -  $0.4 < R < 0.7$  (Figure 21, right panel). The [OIII] luminosities

of these highly extended Seyfert 1's are in the lower  $\sim 50$  percentile of the  $\log P_{[OIII]}$  distribution of the sample, but their  $H\beta$  luminosities are in the upper  $\sim 50$  percentile of the  $\log P_{H\beta}$  distribution. Their  $R$  values are therefore low and they are all classified as Seyfert 1.2's. It is clear that some factor other than the relative orientation of the nuclear obscuring torus to the line of sight affects the  $R$  value, and that this factor is correlated with the radio extent.

If we ignore the 5–7 highly extended Seyfert 1.2's, the distribution of the other Seyferts in Figure 21 appears consistent with the expectations of the unified scheme. Only two confirmed Seyfert 1.0's (Mrk 335 and NGC 4593) have been imaged at high resolution in the radio and both of these are unresolved (two of the Seyfert 1's, NGC 235A and Mrk 231, are of unknown intermediate type). The small number of Seyfert 1.8's and 1.9's limits any conclusions, though it is interesting that all of these are radio-extended and that the 6 Seyfert 1.9's tend to be more radio-extended than the 3 Seyfert 1.8's. In fact, the Seyfert 1.9's appear to be among the most radio extended objects in the sample, even though their  $[OIII]$  and  $H\beta$  luminosities are not significantly different from those of Seyfert 2.0's. Among Seyfert 2.0's, the radio extent and  $R$  are uncorrelated.

## 6. Summary

We have carried out a high resolution radio imaging survey of a sample of early-type Seyfert galaxies. We have presented radio maps and derived properties for all newly observed galaxies. The data forms part of a homogeneous database of a magnitude and distance-limited sample; most galaxies in the sample have been previously imaged in the  $[OIII]$  and  $H\alpha+[NII]$  emission-lines and in continuum (green and red) emission.

The radio luminosities of Seyfert 1's (i.e. Seyfert 1.0's, 1.2's and 1.5's) and Seyfert 2.0's in the early-type sample are similar, and are independent of morphological type within the limited range of morphological type in the sample. However, the fraction of resolved radio sources is larger in the Seyfert 2.0's (93%), than in the Seyfert 1's (64%). The statistical results on Seyfert 1's are limited by the small size of the sample, but their radio and emission-line luminosities are correlated, as found in earlier studies. For Seyfert 2.0's, we find that the emission-line axis on the  $\simeq 10''$  scale tends to align with both the nuclear radio axis measured on a smaller scale and the galaxy disk axis measured on a larger scale. These alignments are consistent with a picture in which the ionized gas lies preferentially in the plane of the galaxy disk. This ambient gas is ionized by nuclear radiation that escapes along and around the radio axis and is compressed in shocks driven by the radio ejecta or by larger-scale winds coaxial with the radio ejecta. We have used the radio -

emission-line alignment to place a constraint on the product of the velocity of the radio ejecta and the period,  $P$ , of any large angle precession of the inner accretion disk and jet :  
 $V_{ejecta} \times P \geq 2 \text{ kpc}$ .

We have also investigated the relationship between the radio extent and  $R = F_{[OIII]}/F_{H\beta}$  ( $F_{H\beta}$  is the total [broad plus narrow]  $H_{\beta}$  flux) for a larger sample of Seyferts. Remarkably, we find that the 5 highly extended ( $\geq 1.5 \text{ kpc}$ ) Seyfert 1's all have  $R$  values in the range  $0.4 < R < 0.7$ , leading to a classification of Seyfert 1.2. This result implies that the value of  $R$ , and hence the Seyfert intermediate type classification, depends on some factor other than the angle between the axis of the obscuring torus and the line of sight. The distribution of the remainder of the Seyferts is consistent with the expectations of the unified scheme.

NN would like to acknowledge Steven White's guidance with all things AIPS, and Pierre Ferruit for useful comments on the manuscript. The National Radio Astronomy Observatory is a facility of the National Science Foundation operated under cooperative agreement by Associated Universities, Inc. This research has made use of the NASA/IPAC extragalactic database (NED) which is operated by the Jet Propulsion Laboratory, Caltech, under contract with the National Aeronautics and Space Administration. We have made use of the Lyon-Meudon Extragalactic Database (LEDA) supplied by the LEDA team at the CRAL-Observatoire de Lyon (France). We have used the Digital Sky Surveys (DSS) which were produced at the Space Telescope Science Institute under U.S. Government grant NAG W-2166. The images of these surveys are based on photographic data obtained using the Oschin Schmidt Telescope on Palomar Mountain and the UK Schmidt Telescope. The plates were processed into the present compressed digital form with the permission of these institutions. This research has made use of the statistical tests in ASURV 1.2 (Lavalley et al. 1992). This work was supported by grant AST 9527289 from NSF and grant NAG 81027 from NASA.

## REFERENCES

- Acosta-Pulido, J. A., Vila-Viraró, B., Pérez-Fournon, I., Wilson, A. S., & Tsvetanov, Z. I. 1996, *ApJ*, 464, 177
- Antonucci, R. R. J. 1993, *ARA&A*, 31, 473
- Argyle, R. W., & Eldridge, P. 1990, *MNRAS*, 243, 504
- Arribas, S., Mediavilla, E., Garcia-Lorenzo, B., & del Burgo, C. 1997, *ApJ*, 490, 227
- Baars, J. W. M., Genzel, R., Pauliny-Toth, I. I. K., & Witzel, A. 1977, *A&A*, 61, 99
- Baum, S. A., O’Dea, C. P., Dallacassa, D., de Bruyn, A. G., & Pedlar, A. 1993, *ApJ*, 419, 553
- Bicknell, G. V., Dopita, M. A., Tsvetanov, Z. I., & Sutherland, R. S. 1998, *ApJ*, 495, 680
- Boksenberg, A. et al. 1995, *ApJ*, 440, 151
- Bower, G., Wilson, A. S., Morse, J. A., Gelderman, R., Whittle, M., & Mulchaey, J. 1995, *ApJ*, 454, 106
- Bower, G., Wilson, A. S., Mulchaey, J., Miley, G. K., Heckman, T. M., & Krolik, J. H. 1994, *AJ*, 107, 1686
- Buta, R., & Purcell, G. B. 1998, *AJ*, 115, 484
- Capetti, A., Axon, D. J., Macchetto, F., Sparks, W. B., & Boksenberg, A. 1996, *ApJ*, 469, 554
- Clements, E. D. 1981, *MNRAS*, 197, 829
- Clements, E. D. 1983, *MNRAS*, 204, 811
- Colbert, E. J., Baum, S. A., Gallimore, J. F., O’Dea, C. P., & Christensen, J. A., 1996, *ApJ*, 467, 551
- Condon, J. J., & Mitchell, K. J. 1984, *ApJ*, 276, 472
- Corwin et al. 1998, The Extended Southern Galactic Catalog, to be published; data accessed from LEDA (ESGC)
- de Bruyn A. G., & Wilson, A. S. 1978, *A&A*, 64, 433

- de Vaucouleurs, G., de Vaucouleurs, A., Corwin, H. G., Buta, R. J., Paturel, G., & Fouque, P. 1991, *Third Reference Catalogue of Bright Galaxies* (Springer-Verlag) (RC3)
- Edelson, R. A. 1987, *ApJ*, 313, 651
- Falcke, H., Wilson, A. S., & Simpson, C. 1998, *ApJ*, in press
- Garnier R., Paturel G., Petit C., Marthinet M. C., & Rousseau J. 1996, *A&AS*, 117, 467
- Giuricin, G., Mardirossian, F., Mezzetti, M., & Bertotti, G. 1990, *ApJS*, 72, 551
- Haniff, C. A., Wilson, A. S., & Ward, M. J. 1988, *ApJ*, 334, 104
- Haniff, C. A., Ward, M. J., & Wilson, A. S., 1991, *ApJ*, 368, 167
- Heckman, T. M., Sancisi, R., Balick, B., & Sullivan, W. T. 1982, *MNRAS*, 199, 425
- Helou, G., Madore, B. F., Schmitz, M., Bica, M. D., Wu, X., & Bennett, J. 1991, in *Databases and On-Line Data in Astronomy*, ed. D. Egret & M. Albrecht (Dordrecht Kluwer), 89 (NED)
- Hewitt, A. & Burbidge, G. 1991, *ApJS*, 75, 297
- Ho, L. C., Filippenko, A. V., Sargent, W. L., & Peng, C.Y. 1997, *ApJS*, 112, 391
- Huchra, J. P. 1989, private communication
- Keel, W. C. 1996, *AJ*, 111, 696
- Kormendy, J., & Richstone, D. 1995, *ARA&A*, 33, 581
- Kukula, M. J., Ghosh, T., Pedlar, A., Schilizzi, R. T., Miley, G. K., de Bruyn, A. G., & Saikia, D. J. 1993, *MNRAS*, 264, 893
- Kukula, M. J., Holloway, A. J., Pedlar, A., Meaburn, J., Lopez, J. A., Axon, D. J., Schilizzi, R. T., & Baum, S. A. 1996, *MNRAS*, 280, 1283
- Kukula, M. J., Pedlar, A., Baum, S. A., & O’Dea, C. P. 1995, *MNRAS*, 276, 1262
- Lauberts, A. 1982, *The ESO/Uppsala Survey of the ESO(B) Atlas*, European Southern Observatory (ESO)
- Lavalley, M., Isobe, T., & Feigelson, E. 1992, in *Astronomical Data Analysis Software and Systems I*, A.S.P. Conference Series Vol. 25, ed. Worrall, D., Biemesderfer, C., & Barnes, J., 245



- MacKenty, J. W. 1990, *ApJS*, 72, 231
- Maia, M. A. G., Da Costa, L. N., Willmer, C., Pelligrini, P. S., & Rite, C. 1987, *AJ*, 93, 546
- Maiolino, R., & Rieke, G. H. 1995, *ApJ*, 454, 95
- Miyaji, T., Wilson, A. S., & Pérez-Fournon, I. 1992, *ApJ*, 385, 137
- Mulchaey, J. S., & Wilson, A. S. 1995, *ApJ*, 455, L17
- Mulchaey, J. S., Wilson, A. S., Bower, G. A., Heckman, T. M., Krolik, J. H., & Miley, G. K. 1994, *ApJ*, 433, 625
- Mulchaey, J. S., Wilson, A. S., & Tsvetanov, Z. 1996a, *ApJS*, 102, 309 (MWZ)
- Mulchaey, J. S., Wilson, A. S., & Tsvetanov, Z. 1996b, *ApJ*, 467, 197
- Nagar, N. M., & Wilson, A. S. 1999, *ApJ*, 516 #1, xx
- Neff, S. G., & de Bruyn, A. G. 1983, *A&A*, 128, 318
- Nilson, P. 1973, *Uppsala General Catalogue of Galaxies*, Royal Society of Sciences of Uppsala (UGC)
- Osterbrock, D. E., & Shaw, R. A. 1988, *ApJ*, 327, 89
- Paturel, G., et al. 1997, *A&AS*, 124, 109 (LEDA)
- Pedlar, A., Kukula, M. J., Longley, D. P. T., Muxlow, T. W. B., Axon, D. J., Baum, S., O’Dea, C., & Unger, S. W. 1993, *MNRAS*, 263, 471
- Perley, R. A., Bridle, A. H., & Willis, A. G. 1984, *ApJS*, 54, 291
- Peterson, B. M., et al. 1991, *ApJ*, 368, 119
- Pogge, R. W. 1989, *ApJ*, 345, 730
- Pringle, J. E. 1997, *MNRAS*, 292, 136
- Rush, B., Malkan, M. A., & Edelson, R. A. 1996, *ApJ*, 473, 130
- Schmitt, H. & Kinney, A. L. 1996, *ApJ*, 463, 498
- Schmitt, H. R., Kinney, A. L., Storchi-Bergmann, T., & Antonucci, R. 1997, *ApJ*, 477, 623, and Erratum *ApJ*, 485, 434 (S97)

- Simpkin, S. M., van Gorkom, J., Hibbard, J., & Hong-Jun, S. 1987, *Science*, 235, 1367
- Storchi-Bergmann, T., Rodriguez-Ardila, A., Schmitt, H. R., Wilson, A. S., & Baldwin, J. A. 1996, *ApJ*, 472, 83
- Takase, B., & Miyauchi-Isobe, N. 1987, *Ann. Tokyo Astron. Obs.*, 21, 251
- Thompson, A. R., Clark, B. G., Wade C. M., & Napier, P. J. 1980, *ApJS*, 44, 151
- Thompson, I. B., & Martin, P. G. 1988, *ApJ*, 330, 121
- Ulvestad, J. S., Antonucci, R. R. J., & Goodrich, R. W. 1995, *AJ*, 109, 81
- Ulvestad, J. S., Roy, A. L., Colbert, E. J. M., & Wilson, A. S. 1998, *ApJ*, in press
- Ulvestad, J. S., & Wilson, A. S. 1983, *ApJ*, 264, L7
- Ulvestad, J. S., & Wilson, A. S. 1984a, *ApJ*, 278, 544 (Paper V)
- Ulvestad, J. S., & Wilson, A. S. 1984b, *ApJ*, 285, 439 (Paper VI)
- Ulvestad, J. S., & Wilson, A. S. 1989, *ApJ*, 343, 659 (Paper VII)
- Unger, S. W., Lawrence, A., Wilson, A. S., Elvis, M., & Wright, A. E. 1987a, *MNRAS*, 228, 521
- Unger, S. W., Pedlar, A., Axon, D. J., Whittle, M., Meurs, E. J. A., & Ward, M. J. 1987b, *MNRAS*, 228, 671
- Urry, M. C., & Padovani, P. 1995, *PASP*, 107, 803
- Veilleux, S. 1991, *ApJ*, 369, 331
- Veilleux, S. & Osterbrock, D. 1987, *ApJS*, 63, 295
- Véron-Cetty, M. P. & Véron, P. 1991, *ESO Sci. Rept.*, No. 10 (Garching: ESO)
- Véron-Cetty, M. P. & Véron, P. 1996, *ESO Sci. Rept.*, No. 17, 1 (Garching: ESO)
- Whittle, M. 1985, *MNRAS*, 213, 33
- Whittle, M. 1992a, *ApJS*, 79, 49
- Whittle, M. 1992b, *ApJ*, 387, 109
- Whittle, M. 1992c, *ApJ*, 387, 121

- Whittle, M., Haniff, C. A., Ward, M. J., Meurs, E. J. A., Pedlar, A., Unger, S. W., Axon, D. J., & Harrison, B. A. 1986, MNRAS, 222, 189
- Whittle, M., Pedlar, A., Meurs, E. J. A., Unger, S. W., Axon, D. J., & Ward, M. J. 1988, ApJ, 326, 125
- Wilson, A. S., & Baldwin, J. 1985, ApJ, 289, 124
- Wilson, A. S., Baldwin, J. A., & Ulvestad, J. S. 1985, ApJ, 291, 627
- Wilson, A. S., & Tsvetanov, Z. I. 1994, AJ, 107, 1227
- Wilson, A. S., & Ulvestad, J. S. 1982, ApJ, 260, 56
- Wilson, A. S., & Ulvestad, J. S. 1987, ApJ, 319, 105
- Wilson, A. S., & Willis, A. G. 1980, ApJ, 240, 429
- Winkler, H. 1992, MNRAS, 257, 677
- Wrobel, J. M., & Heeschen, D. S. 1984, ApJ, 287, 41

TABLE 1  
GALAXIES OBSERVED WITH THE VLA

Name	Other	R.A.	Dec.	Host	Sey	Radio	S <sub>3.6</sub>	S <sub>20</sub>	Radio	T	V	Comments
(1)	(2)	(B1950)	(B1950)	Type	Type	Struct.	(mJy)	(mJy)	Ext. (kpc)	(11)	(km s <sup>-1</sup> )	(13)
		(3)	(4)	(5)	(6)	(7)	(8)	(9)	(10)		(12)	(13)
Mkn 335	...	00 03 45.23	+19 55 28.8	S0/a	1.0	U	2.0	6.8	<0.07,<0.45	0	7688	g,n
Mkn 938	NGC 34	00 08 33.40	-12 23 08.9	Epec	-	S	7.5	55.1	0.17	99	5850	a
NGC 235A	ESO 474-G16	00 40 24.32	-23 48 53.6	S0pec	1?	(L)	2.0	38.5	(1.43)	-2	6692	m
Mkn 348	NGC 262	00 46 04.86	+31 41 04.5	SA0/a	2	L	238.0	302.2	0.05	0(.4)	4410	k
NGC 424	TOL 0109-383	01 09 09.76	-38 20 56.1	SB0/a	2	S	13.1	23.9	0.5	.4(.5)	3300	
Mkn 565	UGC 818	01 13 28.31	+04 01 49.8	SAB0	-	D	0.4	9.0	2.38	-2(.8)	5446	a
NGC 526A	ESO 353-IG66	01 21 37.25	-35 19 33.8	S0pec?	1.9	L	5.0	10.5	8.9	-2	5400	e,q
NGC 513	UGC 953	01 21 37.28	+33 32 21.4	S?	2	S+D	...	41.2	0.62	...	5850	
Mkn 359	UGC 1032	01 24 50.29	+18 55 11.8	SB0pec	1.5	(S)	0.5	2.4	(0.25)	99	5072	n
Mkn 1157	NGC 591	01 30 38.80	+35 24 43.6	SB0/a	2	L	4.9	25.7	0.33	0(.8)	4530	
Mkn 573	UGC 1214	01 41 22.83	+02 05 57.0	SAB0	2	L	1.8	14.3	1.49	-1(.5)	5130	
Mkn 577	UGC 1282	...	...	S0/a	-	...	<0.12	<0.1	...	0(.9)	5220	a
NGC 788	MCG-1-6-25	01 58 36.76	-07 03 25.4	SA0/a	2	(S)	0.7	2.9	(0.2)	0(.6)	4080	
ESO 417-G6	...	02 54 17.01	-32 23 08.8	SA0/a?	2	S	1.0	3.1	1.9	-1(1.7)	4901	
Mkn 1066	UGC 2456	02 56 49.86	+36 37 20.3	SB0	2	L	16.4	96.3	0.72	-1(.8)	3540	
Mkn 607	NGC 1320	03 22 17.77	-03 13 04.8	S0/a	2	U	1.3	3.7	<0.03,<0.19	1(1.2)	2670	
Mkn 612	...	03 28 10.13	-03 18 27.0	SBa:	2	L	2.2	8.2	2.64	0(.6)	6041	
NGC 1358	MCG-1-10-3	03 31 10.77	-05 15 23.9	SAB0/a	2	(S)	0.9	3.4	(0.36)	0(.3)	3870	
NGC 1386	ESO 358-G35	03 34 51.80	-36 09 47.1	Sa/S0	2	S	9.1	28.8	0.03	-6(.5)	810	
ESO 362-G8	MCG-6-12-9	05 09 20.03	-34 27 12.0	S0?	2	(L)	0.8	2.7	(0.47)	0	4830	d
ESO 362-G18	MCG-5-13-17	05 17 44.24	-32 42 27.7	S0/a	1.5	U	2.8	6.0	<0.12,<0.77	-3(.7)	3780	p
NGC 2110	MCG-1-15-4	05 49 46.38	-07 28 02.0	SA0/SBa?	2	L	130.1	289.0	0.93	-3(.8)	2130	
Mkn 3	UGC 3426	06 09 48.20	+71 03 10.3	E2pec	2	L	79.0	1060	0.56	-2(1.1)	4110	
Mkn 620	NGC 2273	06 45 37.63	+60 54 12.8	SAB0/a,SBab	2	L	10.2	52.0	0.18	.5(.5)	1860	
Mkn 6	IC 450	06 45 43.91	+74 29 09.6	SAB0+,Sa	1.5	L	30.0	253	0.82	-5(.6)	5610	n
Mkn 10	UGC 04013	07 43 07.36	+61 03 25.0	SAb,SBbc	1.2	U	...	0.5	<0.64	3(.8)	8753	n,u
Mkn 622	UGC 4229	08 04 21.00	+39 08 58.8	S0:pec	2	S	1.7	6.0	0.80	-2	6840	e
MCG-5-23-16	ESO 434-G40	09 45 28.32	-30 42 59.0	S0	2	S	...	11.0	0.08	-2	2280	b,d,t
Mkn 1239	MCG-0-25-26	09 49 46.29	-01 22 35.7	compact	1.5	U	7.9	56.5	<0.08,<0.59	...	5820	c,n
NGC 3081	ESO 499-IG31	09 57 09.94	-22 35 10.6	SAB0/a	2	(S)	1.0	3.5	(0.38)	0(.3)	2160	
MCG-2-27-9	...	...	...	SB0+pec?	2	...	...	...	...	-1(1.2)	4650	h
NGC 3516	UGC 6153	11 03 22.81	+72 50 20.5	SB0:,SB0/a	1.2	L	4.1	9.4	4	-2(.4)	2700	i,l
NGC 4074	AKN 347	12 01 56.27	+20 35 40.4	S0:pec	2	S	0.8	2.0	0.21	...	6600	
NGC 4117	UGC 7112	12 05 14.13	+43 24 16.1	S0:	2	(L)	<0.1	2.2	(0.33)	-2.3(.6)	958	
NGC 4253	Mkn 766	12 15 55.64	+30 05 25.5	SB0/a:,SBa	1.5	S	8.6	39.3	0.10	1(.6)	3810	j,n
ESO 323-G77	...	13 03 36.56	-40 08 50.0	SAB0	1.2	(L)	1.3	31.9	(1.69)	-2.2(.6)	4470	p
NGC 4968	MCG-4-31-30	13 04 23.92	-23 24 35.1	SAB0	2	U	6.5	32.3	<0.05,<0.30	-2(.8)	2850	
NGC 5077	MCG-2-34-27	13 16 52.93	-12 23 40.7	E	L1.9	U	201.5	207.0	<0.04,<0.23	-5(.4)	2817	a,f
MCG-6-30-15	ESO 383-G35	13 33 01.84	-34 02 25.7	E-S0	1.2	U	0.9	4.0	<0.16,<0.75	-5	2340	d,p
NGC 5252	UGC 8622	13 35 44.34	+04 47 47.2	S0	1.9	L	9.3	17.2	14.79	-2(.8)	6870	r
Mkn 270	NGC 5283	13 39 41.36	+67 55 26.7	SAB0	2	L	3.1	13.9	0.72	-2(1.7)	3090	
NGC 5273	UGC 8675	13 39 55.15	+35 54 21.7	SA0	1.5	S	0.6	2.4	0.43	-2(.3)	1080	i
IC 4329A	ESO 445-G50	13 46 27.87	-30 03 40.9	S0+	1.2	S	10.7	60.0	3.38	-7(.8)	4800	n
NGC 5548	UGC 9149	14 15 43.48	+25 22 01.1	SA0/a,	1.2	L	3.1	23.0	4.45	0(.4)	5100	
ESO 512-G20	MCG-4-35-8	14 42 03.97	-23 35 01.9	SB0+	1	U	1.2	3.6	<0.06,<0.36	-1.3(.9)	3420	o
NGC 6251	UGC 10501	16 37 56.96	+82 38 18.6	E	2	L	651.2	593.0	18.86	-5(.8)	6900	s
IC 5169	ESO 404-G36	22 07 13.38	-36 20 05.3	SAB0+	2	L	3.7	17.6	0.35	-7(.5)	3028	
NGC 7465	UGC 12317	22 59 32.03	+15 41 44.4	SB0:	2	(S)	1.2	6.0	(0.08)	-1.5(.6)	2130	
NGC 7743	UGC 12759	23 41 48.24	+09 39 23.7	SB0+	2	S	0.9	5.3	0.24	-1(.3)	1662	

Comments : a) not a Seyfert galaxy (Sections 2 and 4); b) radio observations from Paper VI; c) radio observations from Ulvestad et al. (1995); d) T is from the ESO Catalog; e) T is from Whittle (1992a); f) Ho et al. (1997) list this galaxy as a Liner of type 1.9; g) host type and T is from NED; h) error in pointing; no useful data; i) Seyfert type from Ho et al. (1997); j) classified as "S" from radio observations in Ulvestad et al. (1995); k) radio structure and extent from Neff & de Bruyn (1983); l) radio extent from Miyaji et al. (1992); m) Seyfert type uncertain, see Section 4; n) Seyfert type from the value of  $F_{[OIII]}/F_{H\beta}$  given by Whittle (1992a); o) Seyfert type from NED; p) Seyfert type from the value of  $F_{[OIII]}/F_{H\beta}$  given by Winkler (1992); q) Seyfert type from Winkler (1992); r) Seyfert type from Acosta-Pulido et al. (1996); s) radio loud object, not included in the early-type Seyfert sample; t) listed as 'S' in Paper VI but no P.A. given and no map published; u) late-type Seyfert.

TABLE 2  
LINEAR SOURCE COMPONENTS

Name	Component	R.A. (B1950)	Dec. (B1950)	S <sub>3.6</sub> (mJy)	S <sub>20</sub> (mJy)	Comment
(1)	(2)	(3)	(4)	(5)	(6)	(7)
NGC 235A	Core	00 40 24.32	-23 48 53.6	2.0	26.5	
NGC 235A	NE	00 40 24.43	-23 48 52.0	...	11.5	
NGC 424	Core	01 09 09.76	-38 20 56.1	12.2	23.9*	
NGC 424	E	01 09 09.86	-38 20 56.1	0.9		
Mrk 565	Core	01 13 28.31	+04 01 49.8	0.4	3.5	
Mrk 565	Ext	...	...	...	5.0	
NGC 526A	Core	01 21 37.26	-35 19 32.2	5.0	5.9	
NGC 526A	NW	01 21 36.79	-35 19 27.5	...	2.5	
NGC 526A	SE	01 21 37.88	-35 19 37.3	...	2.1	
NGC 526B		01 21 39.98	-35 19 45.6	1.0	1.6	
NGC 513	Core	01 21 37.28	+33 32 21.4	...	4.2	
NGC 513	Ext	...	...	...	37.0	
Mrk 1157	NW	01 30 38.79	+35 24 43.9	2.7	25.7*	
Mrk 1157	SE	01 30 38.82	+35 24 43.4	2.2		
Mrk 573	NW	01 41 22.83	+02 05 57.0	0.7	8.9	
Mrk 573	SE	01 41 22.99	+02 05 55.4	0.4	5.4	
Mrk 573	Center	01 41 22.89	+02 05 56.3	0.7		
Mrk 1066	Core	02 56 49.86	+36 37 20.3	4.8	95.3*	
Mrk 1066	Narm	02 56 49.84	+36 37 21.0	5.1		a
Mrk 1066	Sarm	...	...	6.5		
Mrk 612	N	03 28 10.14	-03 18 26.7	1.3	5.6*	
Mrk 612	Center	03 28 10.12	-03 18 28.1	0.35		
Mrk 612	S	03 28 10.17	-03 18 30.8	0.5	2.6	
ESO 362-G8	Core	05 09 20.03	-34 27 12.0	0.4	2.7	
ESO 362-G8	Narm	05 09 20.02	-34 27 11.1	0.4	...	
NGC 2110	Core	05 49 46.38	-07 28 02.0	81.2	289.0*	
NGC 2110	Narm	05 49 46.39	-07 28 00.4	33.2		a
NGC 2110	Sarm	05 49 46.37	-07 28 03.5	15.7		a
Mrk 3	Core	06 09 48.20	+71 03 10.3	50.1	1060*	
Mrk 3	E1	06 09 48.31	+71 03 10.2	7.5		
Mrk 3	E2	06 09 48.49	+71 03 10.4	20.5		
Mrk 620	Core	06 45 37.63	+60 54 12.8	7.6	52.0*	
Mrk 620	W	06 45 37.50	+60 54 12.9	2.6		
Mrk 6	S	06 45 43.91	+74 29 09.6	19.2	235*	
Mrk 6	N	06 45 43.90	+74 29 10.7	8.5		
Mrk 6	SW	06 45 43.90	+74 29 09.2	2.3		
Mrk 6	Ext	...	...	...	18.0	
NGC 4117	S	12 05 14.13	+43 24 16.0	...	1.6	
NGC 4117	N	12 05 14.12	+43 24 19.5	...	0.6	
NGC 5252	Core	13 35 44.34	+04 47 47.2	7.9	13.5	
NGC 5252	N	13 35 44.11	+04 48 09.1	1.4	3.7	
Mrk 270	SW	13 39 41.36	+67 55 26.7	1.6	7.5	
Mrk 270	NE	13 39 41.69	+67 55 28.2	1.5	6.4	
NGC 5548	Core	14 15 43.48	+25 22 01.1	3.1	6.0	
NGC 5548	Narm	14 15 43.39	+25 22 06.5	...	11.5	a
NGC 5548	Sarm	14 15 43.52	+25 21 57.8	...	5.5	a
NGC 6251	Core	16 37 56.97	+82 38 18.5	651.2	498.0	
NGC 6251	Jet	...	...	...	95.0	
IC 5169	S	22 07 13.38	-36 20 05.3	1.6	17.6*	
IC 5169	N	22 07 13.41	-36 20 04.1	2.1		

\* Total flux of this component and all components following it for which the flux value is left blank.

A value of "..." for the flux implies that the component has not been detected at this frequency

Comments : a) position of peak emission.

TABLE 3  
EARLY-TYPE SEYFERTS : RADIO AND OPTICAL P.A.'s

Name (1)	Sey (2)	3.6cm (3)	20cm (4)	Radio (5)	[OIII] (6)	H $\alpha$ + [NII] (7)	Green (8)	Galaxy (9)	Comment (10)
NGC 235A	1?	...	43 a	43 a	77	82	106	117 c	4,8
Mrk 348	2	...	...	170 a	12	59	111	170 a	3,6
NGC 424	2	96 b	96 b	96 b	...	...	...	60 a	4
NGC 526A	1.9	...	128 a	128 a	123	149	100	60 c	7
NGC 513	2	...	167 b	167 b	(53)	67	54	75 a	4
Mrk 359	1.5	80 c	69 c	75 c	...	105	14	10 b	4,9
Mrk 1157	2	151 a	159 a	151 a	150	(108)	108	5 b	4
Mrk 573	2	124 a	126 a	125 a	125	130	101	- d	7
NGC 788	2	...	62 c	62 c	(105)	(75)	112	125 c	7,9
ESO 417-G6	2	0 b	6 b	0 b	140	155	130	- d	7
Mrk 1066	2	130 a	137 a	134 a	134	...	137	90 b	4
Mrk 612	2	10 a	172 a	10 a	...	...	...	- d	7
NGC 1358	2	...	120 c	120 c	131	134	(13)	- d	7,9
NGC 1386	2	170 b	...	170 b	1	11	21	25 a	4
ESO 362-G8	2	165 b	...	165 b	163	177	164	167 a	4,8
NGC 2110	2	10 a	9 a	10 a	177	167	162	161 a	5
Mrk 3	2	86 a	85 a	86 a	113	106	30	- d	7
Mrk 620	2	96 a	95 a	96 a	...	118	92	50 b	4
Mrk 6	1.5	178 a	177 b	178 a	165	...	130	130 b	4
Mrk 622	2	...	0 b	0 b	...	...	144	- d	7
NGC 3081	2	170 c	158 c	158 c	...	125	...	- d	7,9
NGC 3516	1.2	...	8 b	10 a	32	35	10	55 a	1,11
NGC 4074	2	131 b	135 c	131 b	...	99	105	127 b	7
NGC 4117	2	...	177 b	177 b	24	22	17	18 a	4,8
NGC 4253	1.5	160 c	169 c	27 b	112	107	66	60 c	7,10
ESO 323-G77	1.2	40 b	24 c	35 b	6	166	61	155 b	4,8
NGC 5252	1.9	171 a	171 a	171 a	175	...	5	10 b	4
Mrk 270	2	51 a	48 a	50 a	99	94	114	- d	7
NGC 5273	1.5	170 c	179 c	5 b	...	...	...	10 b	2,4
IC 4329A	1.2	...	97 b	97 b	36	135	42	45 a	4
NGC 5548	1.2	...	168 a	168 a	140	45	125	- d	7
IC 5169	2	16 a	...	16 a	...	35	24	22 a	4
NGC 7465	2	32 c	...	32 c	158	(64)	154	- d	7,9
NGC 7743	2	...	21 b	21 b	...	...	...	80 b	4

Note: Values in brackets are uncertain.  
Comments : 1) radio P.A. from Miyaji et al. (1992); 2) radio P.A. from Paper VI; 3) radio P.A. from Neff & de Bruyn (1983); 4) galaxy P.A. from RC3; 5) galaxy P.A. from Wilson & Baldwin (1985); 6) galaxy P.A. from HI 21 cm kinematics (Simpkin et al. 1987); 7) galaxy P.A. measured from DSS; 8) radio classification of source is '(L)'; 9) radio classification of source is '(S)'; 10) radio P.A. from Kukula et al. (1995); 11) galaxy P.A. from UGC.

TABLE 4  
EXPLANATION OF P.A. QUALITY FLAGS

Quality Flag	Radio structure P.A. and extent	Galaxy major axis P.A.
a	'L' radio sources	Kinematic major axis from HI 21 cm, optical absorption-line or emission-line measurements; P.A. from RC3 with $\log R_{25} \geq 0.3$ ; P.A. from UGC or ESO with $a/b \geq 2$ ; galaxy not listed in RC3, UGC and ESO, but DSS measurements give $a/b \geq 2$ .
b	'S' radio sources with high S/N ratio	P.A. from RC3 with $0.04 \leq \log R_{25} < 0.3$ ; P.A. from UGC or ESO with $1.1 \leq a/b < 2$ ; galaxy not listed in RC3, UGC and ESO, but DSS measurements give $1.1 \leq a/b < 2$ .
c	'S' radio sources with low S/N ratio or doubtful extension	Galaxy listed in RC3, UGC or ESO with no P.A. and we use a photometric P.A. from other source; evidence of disturbed or peculiar morphology.
d		$\log R_{25} < 0.04$ or $a/b < 1.1$ and/or strongly interacting/highly disturbed/ill-defined.

Notes : (1)  $\log R_{25}$  as defined in RC3; (2)  $a/b$  is the ratio of major axis to minor axis.

TABLE 5  
PARAMETERS FOR VLA CONTOUR PLOTS

Fig. No. (1)	Name (2)	3.6 cm r.m.s. ( $\mu\text{Jy}$ ) (3)	3.6 cm contours (multiples of r.m.s.) (4)	20 cm r.m.s. ( $\mu\text{Jy}$ ) (5)	20 cm contours (multiples of r.m.s.) (6)
1	Mkn 335	66	-4,-2,2,4,6,8,10,15,20,25,30	110	-4,-2,2,4,6,8,10,15,20,30,40,60
1	Mkn 938	71	-4,-2,2,4,6,8,10,15,20,25,30,40,50	110	-4,-2,2,4,6,8,10,20,40,60,100,150,200,300,400
1	NGC 235A	61	-4,-2,2,4,6,10,20,30	130	-4,-2,2,4,6,8,10,15,20,25,30,35,40,45,50,60,80,100,150
2	Mkn 348	76	-6,-4,-2,2,4,6,10,50,100,200,400,800,1200,2400	120	-4,-2,2,4,6,10,20,40,100,250,500,1000,1500,2000
2	NGC 424	150	-4,-2,2,4,6,10,20,40,60	230	-6,-4,-2,2,4,6,8,10,15,30,60,90
2	Mkn 565	36	-6,-4,-2,2,4,6	73	-4,-2,2,4,6,8,10,15
3	NGC 526A	71	-5,-2,2,5,10,20,40	92	-6,-4,-2,2,4,6,8,10,15,20,25,30,40,50
3	NGC 513			69	-6,-4,-2,2,4,6,8,10,15,20,25,30,40
3	Mkn 359	42	-4,-2,2,4,6,8,10	150	-2,2,4,6,8,10
4	Mkn 1157	68	-4,-2,2,4,6,10,15,20	90	-4,-2,2,5,10,20,50,90,140,190
4	Mkn 573	55	-4,-2,2,4,6,8,10	180	-4,-2,2,4,6,8,10,15,20,25,30
4	NGC 788	46	-4,-2,2,4,6,8,10	88	-4,-2,2,4,6,8,10,15,20,25
5	ESO 417-G6	65	-4,-2,2,4,6,8,10,14	140	-8,-6,-4,-2,2,4,6,8,10
5	Mkn 1066	90	-4,-2,2,4,6,8,10,15,30	120	-4,-2,2,4,6,10,20,40,80,120,150,200,250,280
5	Mkn 607	73	-4,-2,2,4,6,8,10,12,14	69	-4,-2,2,4,6,8,10,15,20,25,30,40
6	Mkn 612	36	-4,-3,-2,2,3,4,5,6	67	-4,-2,2,4,6,8,10,12,15,20,40
6	NGC 1358	94	-4,-2,2,4,6,8	110	-4,-2,2,4,6,8,10,15,20
6	NGC 1386	100	-6,-4,-2,2,4,6,10,20,40,60,80	180	-4,-2,2,4,6,10,20,30,40,60,80,120,140
7	ESO 362-G8	57	-4,-2,2,3,4,5,6	140	-4,-2,2,4,6,8,10,12,14
7	ESO 362-G18	120	-4,-2,2,4,6,10,15,20	190	-4,-2,2,4,6,8,10,15,20,25
7	NGC 2110	100	-10,-6,-4,-2,2,4,6,10,15,30,45,90,180,300,600	360	-6,-4,-2,2,4,6,10,20,40,60,80,100,150,200,250
8	Mkn 3	330	-6,-4,-2,2,4,6,10,15,20,30,40,70,100	380	-10,-4,-2,2,4,10,20,60,100,200,300,400,600,1200,1800
8	Mkn 620	69	-4,-2,2,4,6,8,10,12,20,40,80	140	-4,-2,2,4,6,8,10,20,40,60,80,100,150,200
8	Mkn 6	56	-6,-4,-2,2,4,6,10,30,60,90,120,150	170	-4,-2,2,4,6,10,20,40,100,200,500,800
9	Mkn 10			52	-4,-2,2,4,6,8
9	Mkn 622	80	-4,-2,2,4,6,8,10,14,18	91	-4,-2,2,4,6,8,10,15,20,25,30,35
9	NGC 3081	50	-4,-2,2,4,6,8,10,12	100	-4,-2,2,4,6,8,10,15,20
10	NGC 3516	87	-4,-2,2,4,6,10,20,30,40	150	-6,-4,-2,2,4,6,8,10,15,20,25,30,35
10	NGC 4074	42	-4,-2,2,4,6,8,10	85	-4,-2,2,4,6,8,10,15,20
10	NGC 4117	31	-4,-2,2,4,6	74	-5,-4,-3,-2,2,3,4,5,6,7
11	NGC 4253	61	-4,-2,2,4,6,10,20,40,60	180	-4,-2,2,4,6,10,20,40,60,80,100,140,180
11	ESO 323-G77	76	-3,-2,2,3,4,5,6,8	270	-6,-4,-2,2,4,6,8,10,15,20,25,30,40,50,60
11	NGC 4968	65	-4,-2,2,4,6,10,20,40,60,80	120	-4,-2,2,4,6,10,20,40,60,80,100,150,200
12	NGC 5077	83	-10,-4,-2,2,4,10,50,100,500,1000,1500,2000	180	-4,-2,2,4,6,10,20,40,60,100,200,300,400,500,600,800,1000
12	MCG-6-30-15	69	-4,-2,2,4,6,8,10	300	-4,-2,2,4,6,8
12	NGC 5252	70	-6,-4,-2,2,4,6,10,20,40,60,80,100,150,200	86	-4,-2,2,4,6,10,20,30,40,70,110
13	Mkn 270	43	-4,-2,2,4,6,8,10,15,20	93	-4,-2,2,4,6,8,10,15,20,25,30,40,50,60
13	NGC 5273	53	-4,-2,2,4,6	81	-4,-2,2,4,6,8,10,15,20
13	IC 4329A	65	-4,-2,2,4,10,20,40,80,150	200	-6,-4,-2,2,4,6,8,10,15,20,30,40,60,80,100,150,200
14	NGC 5548	88	-4,-2,2,4,6,8,10,15,20,25,30	91	-4,-2,2,4,6,8,10,12,15,20,40,60
14	ESO 512-G20	76	-4,-2,2,4,6,8,10,12	100	-4,-2,2,4,6,8,10,15,20,25,30,35
14	NGC 6251	200	-6,-4,-2,2,4,6,15,30,100,200,400,800,1500,2400	270	-6,-4,-2,2,4,6,10,20,30,40,100,500,1000,1500
15	IC 5169	88	-6,-4,-2,2,4,6,8,10,12,14	190	-4,-2,2,4,6,8,10,15,20,25,30,40,50,60
15	NGC 7465	59	-4,-2,2,4,6,8	110	-2,2,4,6,8,10,15,20,25,30,40
15	NGC 7743	71	-4,-2,2,4,6,8,10	81	-4,-2,2,4,6,8,10,15,20,25,30,40

Notes : Negative contours are plotted with dashed lines. The most negative contour is lower than the lowest flux on the map; it is listed so that the lowest flux can be estimated from the contour map.

Columns : (1) figure number; (2) galaxy name; (3) r.m.s. noise ( $\mu\text{Jy}$ ) in 3.6 cm image; (4) contour levels in 3.6 cm image in multiples of the r.m.s. noise; (5) r.m.s. noise ( $\mu\text{Jy}$ ) in 20 cm image; (6) contour levels in 20 cm image in multiples of the r.m.s. noise.



TABLE 6  
RESULTS OF UNIVARIATE STATISTICAL COMPARISONS

Property (1)	Distribution A (2)	Distribution B (3)	Gehan 1 (4)	Gehan 2 (5)	Logrank (6)	Figure Number (7)
Fraction of resolved radio sources	1	2.0	.013	.013	.013	17c
Mean radio extent	1	2.0	.92	.92	.44	17e,f
Mean log P <sub>20</sub>	1	2.0	.40	.41	.46	17a
$P.A._{Radio} - P.A._{[OIII]}$	1	2.0	.15	.17	.22	18
	1	uniform	.50	.48	.55	
	2.0	uniform	.0021	.0001	.0001	
$P.A._{Radio} - P.A._{H\alpha}$	1	2.0	.032	.044	.12	18
	1	uniform	.99	.99	.61	
	2.0	uniform	.011	.0037	.0021	
$P.A._{[OIII]} - P.A._{H\alpha}$	1	2.0	.82	.81	.98	20
	1	uniform	.041	.0064	.31	
	2.0	uniform	.0001	<.0001	.0001	
$P.A._{[OIII]} - P.A._{Green}$	1	2.0	.35	.36	.92	20
	1	uniform	.027	.0098	.0021	
	2.0	uniform	.0025	.0002	.012	
$P.A._{[OIII]} - P.A._{Galaxy\ major\ axis}$	1	2.0	.31	.33	.61	20
	1	uniform	.12	.081	.021	
	2.0	uniform	.0097	.0015	.015	
$P.A._{H\alpha} - P.A._{Green}$	1	2.0	.069	.082	.18	20
	1	uniform	.95	.95	.40	
	2.0	uniform	.0016	.0001	.029	
$P.A._{H\alpha} - P.A._{Galaxy\ major\ axis}$	1	2.0	.18	.20	.15	20
	1	uniform	.80	.79	.36	
	2.0	uniform	.0091	.0016	.0083	
$P.A._{Green} - P.A._{Galaxy\ major\ axis}$	1	2.0	.62	.62	.97	...
	1	uniform	.0053	<.0001	.044	
	2.0	uniform	.0002	<.0001	<.0001	

Columns : (1) property tested; (2) and (3) the two distributions being compared. '1' represents type 1 Seyferts, '2.0' represents type 2.0 Seyferts and 'uniform' represents a uniform distribution; (4) result of Gehan's test with permutation variance; (5) result of Gehan's test with hypergeometric variance; (6) result of the logrank test; the values listed in columns (4), (5) and (6) represent the probability that Distribution A and Distribution B are drawn from the same parent population; (7) figure number of plot.

All results involving Seyfert 1's are unreliable because of the limited number ( $\sim 8-10$ ) of galaxies available.

TABLE 7  
RESULTS OF BIVARIATE STATISTICAL COMPARISONS

Variable A (1)	Variable B (2)	Seyfert Type (3)	Cox (4)	Kendall $\tau$ (5)	Spearman $\rho$ (6)	Figure Number (7)
P <sub>20</sub>	Radio struct.	1	.34	.43	.44	17d
		2.0	.024	.023	.022	
P <sub>20</sub>	Radio extent	1	.12	.20	.21	17e,f
		2.0	.21	.050	.034	
P <sub>20</sub>	L <sub>[O III]</sub>	1	.006	.013	.023	19a
		2.0	.14	.15	.18	
P <sub>20</sub>	L <sub>H<math>\alpha</math></sub>	1	.006	.011	.029	19b
		2.0	.19	.59	.57	

Columns: (1) and (2) the two variables being compared; (3) Seyfert type. '1' represents type 1 Seyferts and '2.0' represents type 2.0 Seyferts; (4) result of the Cox proportional hazard test; (5) result of the generalized Kendall's  $\tau$  test; (6) result of Spearman's  $\rho$  test; the values listed in columns (4), (5) and (6) represent the probability that a correlation is not present between variable A and variable B; (7) figure number of plot.

All results involving Seyfert 1's are unreliable because of the limited number of galaxies available.